Modelling of Non-Equilibrium Wet Compression in Compression-Resorption Heat Pumps

Marina Brancaccio

TU Delft

Modelling of Non-Equilibrium Wet Compression in Compression-Resorption Heat Pumps

by

Marina Brancaccio

to obtain the degree of Master of Science
at the Delft University of Technology,
to be defended publicly on Monday October 2, 2023 at 10:00 AM.

Student number:	5609852
Project duration:	December 12, 2022 – October 2, 2023
Thesis committee:	Prof. dr. ir. K. Hooman, TU Delft, supervisor
	Dr. ir. M. Ramdin, TU Delft
	Dr. ir. C. Falsetti, TU Delft

TU Delft

Acknowledgements

These two years in Delft have flown by, in the blink of an eye. During this time, I had the privilege of creating new experiences and learning about different cultures. Nevertheless, there were moments when I longed to return to my beloved homeland. As I reach the end of this incredible journey, there are many people who have contributed to my success and it is only right to recognize their contributions here.

First and foremost, I extend my heartfelt appreciation to my supervisor, prof. Kamel Hooman. Professor Hooman's support, constant availability and insightful discussions have been essential throughout my master thesis journey. I am truly grateful to Professor Carlos Infante Ferreira for his invaluable guidance and mentorship. Professor Ferreira not only introduced me to the intricacies of this complex subject, but generously shared his expertise and knowledge. I would like to thank Dr. ir. Mahinder Ramdin and Dr. ir. Chiara Falsetti for taking the time to review my research thesis and for their presence at my graduation defense.

All of this could not have been possible without my parents. You have not only supported me since the beginning of my academic journey, but you have also inspired me and made me the person I am today. Thank you for always believing in me. You gave me the strength to keep going even in the most hopeless moments. My greatest satisfaction is that I made you proud.

Boaz, I don't know where to even begin. You have helped through my bachelor's degree, during the contest, in every interview and now here once again. Even when you were tired or overwhelmed with your own work, you have never refused to help and to offer your unwavering support. It is clear that you see my success as your own and that is something that I deeply appreciate. Your encouragement and guidance have played a significant role in my journey and I consider myself incredibly fortunate to have you by my side. I could not have done this without you. Thank you for always being there.

I would like to express my gratitude to my family and friends back in Italy. Throughout my journey in the Netherlands, my unwavering desire to reunite with you has been a driving force. Despite the physical distance, your constant support through calls and messages has meant the world to me. I am deeply grateful for your encouragement from Italy and I eagerly wait for the moment we can meet again.

I would like to thank all the friends who have accompanied me on this journey in the Netherlands. I will forever remember every moment we spent together, from the weekly volleyball to the weekend dinners. You brought laughter and joy to my days in P&E, but you have also helped when I was in need. Even when you were overloaded with your thesis projects, you stayed there to listen and gave me new ideas. I couldn't have asked better friends to share this journey with. I will miss you all.

Delft, September 2023
Marina Brancaccio

Abstract

The ever-increasing power demand, the high scarcity of fossil fuel resources and the growing environmental pollution have pushed the development on technologies related to sustainable energy systems. Maximizing the energetic performance of industrial processes is a key aspect in this quest for sustainable energy management. A large share of waste heat below 100°C is rejected into the environment during industrial processes. This low temperature industrial waste heat can be a relevant heat source, reducing the consumption of fossil fuel and the emission of CO_2 into the atmosphere. While these lower temperatures may not be suitable for direct industrial use and their capture may not be economically justified, the implementation of a heat pump allows for the elevation of these stream temperatures to levels that can support a wide range of industrial processes.

Heat pumps can be utilized to upgrade waste heat streams from low to higher temperature levels which can then be used as energy supply for other industrial processes. State-of-the-art heat pumps are still restricted to temperature levels below 120°C due to long payback periods and technical limitations regarding the compressor. The application of heat pumps in industry could become more widespread if the technology would allow for a higher temperature output. Compression-resorption heat pumps (CRHPs) are a promising option to upgrade waste heat streams since they combine the advantages of absorption heat pumps (working with a mixture having non-isothermal phase transitions and low environmental impact) and vapor-compression heat pumps.

CRHPs can operate both under dry and wet compression conditions. One of the main issues in reaching high temperatures with dry compression is the degradation of the oil, which leads to a reduction of the performance. Employing wet compression, the liquid can function as a lubricant avoiding both oil contamination and irreversibility caused by the superheating of the vapor. As pointed out by several researchers, a crucial point for the feasibility of high temperature CRHPs is a good value of isentropic efficiency for the compressor. As such, since a technological solution is currently not commercially available, the diffusion of CRHPs in the industrial processes is inhibited.

This research thesis develops a numerical model of the compressor in which the liquid phase and the vapor phase are at non-equilibrium conditions. The model incorporates heat transfer between the phases, yielding new insights and results. The validated model serves as a tool for analyzing optimal operating conditions to maximize compressor efficiency. A case study within the dairy industry was considered. The results indicate a 60% reduction in operating costs and a saving of 104 tonnes of emissions if a single heat pump substitutes a traditional boiler. The substitution of fossil fuel fired boilers with heat pumps becomes increasingly necessary in light of the EU Renewable Energy Directive, ratified in 2023, which targets a 45% renewable energy share by 2030. The development of such next generation heat pumps could be a major breakthrough for optimizing energy management in industrial processes.

Contents

Nomenclature

A	area [m^2]
C	clearance size [m]
COP	coefficient of performance [-]
cp	specific heat capacity [J kg^{-1} K^{-1}]
D	diameter [m]
h	specific enthalpy [kJ kg^{-1}]
$\dot{m}$	mass flow rate [kg s^{-1}]
n	rotational speed [rpm]
L	length [m]
$\dot{Q}$	rate of heat transfer [kW]
Q	vapor quality [-]
p	pressure [bara]
r	radius [m]
S	slip ratio [-]
U	overall heat transfer coefficient [W m^{-2} K^{-1}]
v	specific volume [m^3 kg^{-1}]
V	volume [m^3]
$\dot{W}$	rate of work transfer [kW]
w	flow velocity [m s^{-1}]
X	ammonia concentration [$kg_{NH3}kg_{sol}^{-1}$]
s	specific entropy [kJ kg^{-1} K^{-1}]
T	temperature [°C]
z	number of lobes [-]

Greek symbols

Δ	difference [-]
δ	liquid thickness [m]
ϵ	void fraction
ζ	flow coefficient [-]

η_{is} isentropic efficiency [-]

η_{vol} volumetric efficiency [-]

ρ density [kg m^{-3}]

ϕ rotor angle [°]

ω angular velocity [rad s^{-1}]

List of Abbreviations

CAPEX Capital expenditure

CFC Chlorofluorocarbons

CRHP Compression-resorption heat pump

GWP Global warming potential

HACHP Hybrid absorption-compression heat pump

HCFC Hydrochlorofluorocarbons

HFC Hydrofluorocarbons

OPEX Operating expenses

PBP Payback period

PEC Purchased equipment cost

TCI Total capital investment

VCHP Vapor-compression heat pump

Subscripts

abs absorber

comp compressor

cw cooling water

des desorber

dis discharge

down downstream

ev evaporated

flash flashed

G gas

HP heat pump

in inlet

ind indicated

is isentropic

L liquid

m	male
max	maximum
mom	momentum
out	outlet
S	solid
sat	saturated
sub	subcooler
suc	suction
up	upstream
vap	vaporization

List of Tables

List of Figures

1 Introduction

Ever since the dawn of the Industrial Revolution in the 18^{th} century, fossil fuels have been massively used to power economic growth. For heating, electricity production and industrial processes, steam has emerged as an essential component in meeting the world energy demand, due to its abundance and relatively low cost.

Russia has been the world's largest exporter of fossil fuels until now, but energy policies have changed since Russia's invasion of Ukraine early 2022, causing a potential turning point towards cleaner energy system. The rise in energy prices and shortage of the global supply of natural gas from Russia are brightening the prospect of growth in the renewable energy sector [International Energy Agency (IEA, 2022b)]. The change is caused both by the limited amount of available fossil fuels and by their effect on climate change. Fossil fuels cause the emission of gases like CO_2, CO and NO_x into the atmosphere, enlarging the greenhouse effect. In order to avoid increasing the effects of global warming like the accelerated rising of sea levels and prolonged and more intensive heat waves, the use of fossil fuels should be reduced and the energetic performance of industrial processes needs to be improved. The consequences of flue gas emission are not limited to climate change though. Particulate matter, causing health issues, is a major issue for urban areas.

In order to cope with depleting energy resources and climate change, an energy transition towards renewable and sustainable energy is necessary. Throughout the last 30 years, many clean and sustainable energy sources have been proposed for the replacement of fossil fuels driven energy sources. Converting natural energy sources like wind, water and light into electricity has been widely investigated and currently many methods are – in theory – able to satisfy a large part of the global energy demand. These technologies do not involve the emission of CO_2 into the atmosphere, and are hence considered as clean or green technologies.

A key-aspect in the transition towards a more sustainable future lies in the replacement of fossil fuel based systems with heat pumps. Although heat pumps consume a considerable amount of electricity, they are considered as renewable energy systems, as they can exploit renewable sources to draw thermal energy from the external environment. As stated by IEA (2022a), heating represents one third of the European Union's gas demand: substituting gas fired boilers by heat pumps is a clear solution to improve energy efficiency and environmental performances. Currently, 43% of the global energy consumption for thermal conversion is used for industrial applications. Of this share, 20-30% is lost through waste heat contained in liquid streams and exhaust flue gas and is rejected into the environment at temperatures below 100°C. Low-temperature industrial waste heat can be a relevant heat source, reducing the consumption of fossil fuels and the global warming effect. Heat pumps are a means to upgrade low temperature waste streams into valuable utility streams.

Compression-resorption heat pumps (CRHPs) are a very promising option to upgrade waste heat streams. While more classic vapor-compression heat pumps (VCHPs) use dry compression, the CRHPs can use wet compression, which is compression in the two-phase region. When dealing with high temperature applications dry compression leads to performance degradation caused by super-

heating of vapor and thermo-chemical instabilities of the lubricant oil. For wet compression applications the liquid itself is used as lubricant, avoiding any contact between operating fluid and oil.

Currently, the use of heat pumps for upgrading waste heat streams is quite limited. Recently, European industrial waste heat theoretical potential accounted to 300 TWh/year, of which one third is lost at temperature levels below 200 °C [Papapetrou et al. (2018)]. Considering that recovering approximately 1 MWh of thermal energy would avoid the emission of 0.202 tonnes of CO_2 into the environment, the impact of such recovery is clear. According to Panayiotou et al. (2017) chemical and petrochemical industry (C&P) and the iron and steel industry (I&S) respectively cover 25.9% and 25.0% of the total waste heat potential. In particular, C&P industry is interesting for heat pump applications since 59.3% of its waste energy share is delivered at low temperature levels [Bianchi et al. (2019)]. Heat at low temperature levels can either be directly used for minor applications or upgraded to higher temperature levels for being used in C&P or other industrial operations. As shown in Table 1.1, heat pumps could be used to produce the heat required in multiple processes, especially when delivering temperatures above 100°C without an exponential increase of the investment and operating costs.

Table 1.1: Summary of industrial process temperatures. Data from Brückner et al. (2015).

Industry	Process	Temperature range (°C)
Food & Beverage	Sterilizing	120 - 150
	Pasteurizing	80 - 110
	Drying	30 - 130
Chemical	Distilling	110 - 300 / 90 - 130
	Others	120 - 180
Textile	Dyeing	100 - 160
	Steaming	100 - 130
Non-metallic mineral process	Drying	35 - 150

In light of the EU Renewable Energy Directive, ratified in 2023, which targets a 45% renewable energy share by 2030, the urgency for the rapid advancement of heat pump technology in industrial applications becomes a significant concern. State of art of heat pumps for high temperature applications is still restricted to temperatures around 100 °C due to high investment costs and technical limitations regarding the compressor. As mentioned before, CRHPs could be a solution for this problem if operating under wet compression conditions. This research study focuses on the development of a compressor model which simulates the compression process of ammonia-water mixture (NH_3-H_2O) for a CRHP working under wet compression conditions.

1.1. Outline

The outline for the rest of the research thesis is organized in the following way:

- *Chapter 2* presents the theoretical background of CRHPs operating in various modes, discusses suitable compressors for this operation and summarizes previous studies on the subject.
- *Chapter 3* defines the research question and outlines the main challenges of the research topic.
- *Chapter 4* presents the experimental setup.
- *Chapter 5* discusses the development of the numerical models.
- *Chapter 6* presents the experimental validation of the numerical models.
- *Chapter 7* delves into the model results obtained from investigating the operating conditions.
- *Chapter 8* outlines the economic and energetic benefits and disadvantages when applying the CRHP in a real-life application.
- *Chapter 9* finalizes the research thesis by presenting the conclusions and recommendations for this research topic.

2

Theoretical background

In this chapter an overview of different types of heat pumps is given. Following a brief summary on the working principle of heat pumps, their technological limits and advantages are analyzed in the context of upgrading waste heat in order to find the most suitable solution. In particular, the widely known vapor-compression heat pump is compared to compression-resorption heat pump, which can be further distinguished in CRHPs with solution recirculation (HACHP) and CRHPs with total wet compression, hereafter referred to as CRHPs. The key aspects to consider when operating under wet and dry compression conditions are drawn and summarized in section 2.2.2. Previous works done on the development of CRHPs using a compressor operating with liquid are reviewed in section 2.3.

2.1. Heat pump: working principle

The heat pump is a thermal machine capable of transferring thermal energy from a lower temperature source to a higher temperature source by administering mechanical energy from the external environment. It carries out a thermodynamic cycle, exploiting the physical principle of evaporation and condensation of a refrigerant fluid. The vapor-compression heat pump consists of the following components:

- Compressor: an operating machine capable of raising the pressure and temperature of a fluid at the expense of mechanical energy supplied from the external environment.
- Condenser: a heat exchanger capable of condensing a substance, or capable of bringing it from the gaseous state to the liquid state, releasing useful heat.
- Expansion valve: a component used for reducing and controlling the pressure of a fluid stream in a duct.
- Evaporator: a heat exchanger designed to obtain the evaporation of a fluid, or to bring it from the liquid state to the gaseous state, absorbing heat.

Summarizing, heat is removed from the low temperature source ($\dot{Q}_{source}$), brought to higher temperature and pressure levels through the use of a compressor performing work ($\dot{W}_{comp}$) and released to the heat sink at high temperature level ($\dot{Q}_{sink}$). As such, energy is conserved.

$$\dot{Q}_{source} + \dot{W}_{comp} = \dot{Q}_{sink} \tag{2.1}$$

The performance of the heat pump is quantified through a parameter named COP (coefficient of performance), expressed as the ratio between the heating output and the work furnished to the cycle. Since the heat pump is able to return a greater energy share than spent this parameter is larger than unity.

$$COP = \frac{\dot{Q}_{sink}}{\dot{W}_{comp}} \tag{2.2}$$

Several parameters influence the COP, between these the temperature lift is predominant. The temperature lift is the difference in temperature between the heat sink and the heat source. The larger this difference, the more energy input is required, leading to a reduction of COP for a fixed energy output. Although VCHPs are very developed, limited temperature lift can be reached due to losses in the compressor while increasing the pressure ratio. On the contrary, compression-resorption heat pumps expand the range of temperature lifts at which heat pumps can work. This was confirmed by Jensen et al. (2015), who compared the technical and economical aspects of HACHPs working with NH_3-H_2O and VCHPs working with R717 (pure ammonia). Results show that HACHPs can extend the range of operating conditions at which the heat pump can work while being economically advantageous. This is especially valid for temperatures at which the heat is supplied above 90°C, where VCHPs working with R717 cannot be applied. With the HACHPs both higher heat supply temperatures and higher temperature lifts can be obtained compared to VCHPs. This is attributed to the lower pressure levels of the zeotropic mixture required to reach specific temperatures.

Compression-resorption heat pumps use the same working principle as conventional heat pumps, however, the condenser and the evaporator are replaced by an absorber and a desorber, respectively. During the absorption and desorption processes heat is extracted and emitted at a non-constant temperature due to changes in composition of the mixture. In the desorber the evaporation is not complete and as such the fluid leaving the desorber is in vapor-liquid phase. Two configurations are possible, based on the way the fluid is handled after desorption : compression-resorption heat pumps with wet compression or compression-resorption heat pumps with solution recirculation, also named hybrid-absorption heat pumps. In the first case, the solution is directly sent to the compressor as a mixture of vapor-liquid and a total wet compression cycle occurs (Figure 2.1).

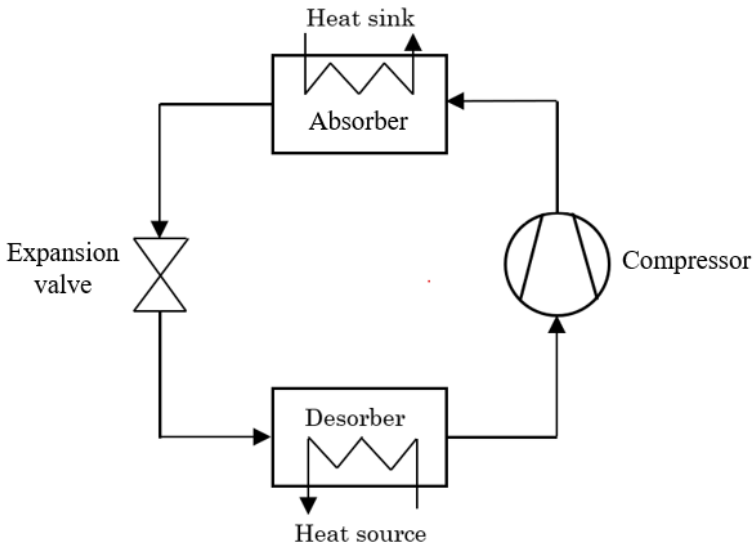

Figure 2.1: Simplified representation of compression-resorption heat pump cycle with wet compression.

In the second case, a separator is placed before the compressor in order to split the liquid phase from the vapor phase. In this way, one stream has a weak solution of ammonia and the other stream has a strong solution of ammonia.

The strong solution, consisting of vapor, is compressed at high temperatures and can lead to pressure levels much higher than those which are necessary for a CRHP under wet compression conditions to reach similar levels, since the superheating zone is not avoided.

The lean solution, consisting of liquid, is pumped in an additional pump to reach the same high pressure at the discharge of the compressor. The liquid exchanges heat with the solution leaving the absorber through an additional heat exchanger, this increases the liquid temperature and lowers the solution temperature at the absorber outlet. The liquid and the vapor phase are combined before entering the absorber.

The working principle of HACHP, based on the Osenbrück cycle, is represented in Figure 2.2.

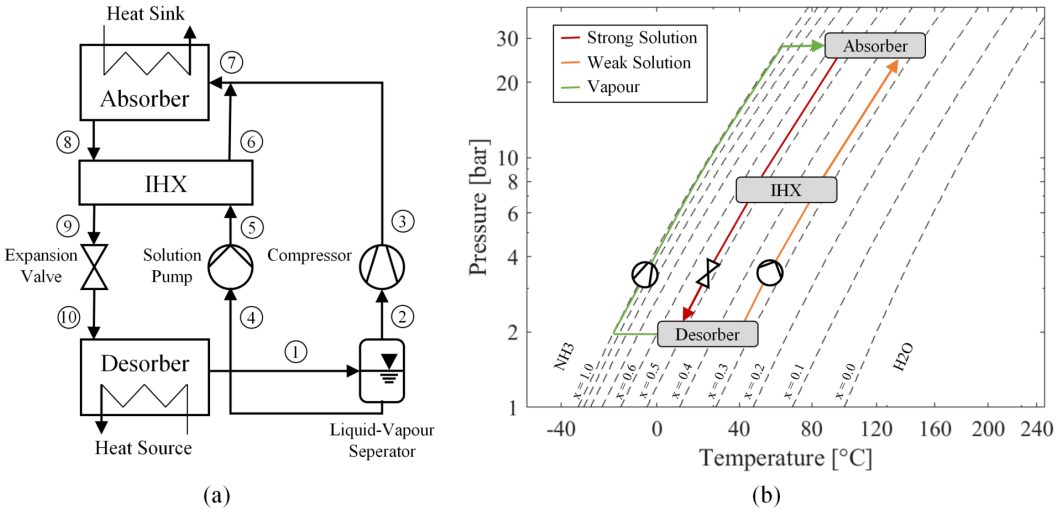

Figure 2.2: (a) Simplified representation of an absorption-compression hybrid heat pump cycle (b) PTX diagram of saturated liquid for an ammonia-water mixture with hybrid heat pump components. Figure from Ahrens et al. (2019).

Additionally, an essential step in mitigating CO_2 emissions consists of substituting high global warming potential (GWP) fluids, usually applied in VCHPs, by environmentally friendly fluids. CRHPs can fulfill this requirement working with NH_3-H_2O. In addition to being natural fluids with no ozone depletion and zero GWP, operating with this mixture shows both higher COP due to non-isothermal phase transition at constant pressure and higher supply temperatures, which are achieved at relatively low operating pressures.

2.2. Heat pump selection for high temperature applications

Several types of heat pumps have been widely investigated as a means for waste heat recovery. Vapor-compression heat pumps have been extensively considered to be a well developed technology. However, they are often constrained by high compressor discharge temperatures and a significant environmental footprint of the refrigerant. As yet, the heat pumps are limited in operating temperature (<120 °C) and temperature lift (<50°C). The application of heat pumps in industry could be remarkably enhanced if the operating temperature would be increased to 130-150 °C or if the temperature lift would be increased to 50-100 °C, as discussed by Mikielewicz and Wajs (2019). HACHPs and CRHPs operating with wet compression are gathering interest because of their theoretical potential to attain higher supply temperatures and higher temperature lifts with a relative good level of COP.

2.2.1. Differences and similarities between CRHPs and VCHPs

Ziegler and Riesch (1993) presented many advantages of CRHPs. The main benefit lies in the use of zeotropic mixtures, which condense and evaporate at non-constant temperatures; in this case an additional degree of freedom is available to control the process. The mixture concentration could be used to reduce the irreversibility in the heat exchangers when trying to match the mixture temperature glide with the external fluid temperature profile. Apart from the phase transition at non-constant temperature, another benefit lies in the replacement of high GWP refrigerants by low GWP refrigerants based on natural fluids, which are not harmful to the ozone layer.

This issue was already described in 1997 by Brunin et al. (1997), in occasion of the production ban of R114 fluid (a chlorofluorocarbon (CFC)). In this study, they analyzed the high temperature operating domains of the two following modes: a VCHP using hydrofluorocarbons (HFC) and a HACHP using NH_3-H_2O with the same characteristics. This work was born from the necessity to find more eco-friendly fluids to operate with compression heat pumps at high temperatures. Hydrofluorocarbons can work at medium temperatures up to 80 °C, however, some issues may occur when they are used at higher temperatures (80-120°C). In addition, they still have an impact on global warming releasing CO_2. In

contrast, HACHPs operating with NH_3-H_2O can cover high temperature applications with a good level of system performance and minimum emissions.

In order to replace conventional boilers which supply hot water in industrial processes, Kim et al. (2013) studied a two-stage compression hybrid heat pump system based on NH_3-H_2O operating with some auxiliary components. In the experiments, different parameters were varied in order to obtain the best operating characteristics. For their system, an ammonia concentration of 0.421 kg/kg in the weak solution enabled the production of hot water higher than 90°C, using both the heat source and the sink at 50°C. Increasing the ammonia concentration higher temperature supply could be achieved, however, the compressor discharge pressure exceeds the technical limit making the operation unfeasible. Since dry compression is performed, the vapor reaches very high discharge temperatures limiting the production of hot water at temperatures lower than 90°C. Here, the benefit of adopting wet compression for high-temperature requirements becomes evident. By compressing in the double phase zone and using an oil-free compressor, the limitations on the compressor temperature would be mitigated. Furthermore, the liquid would serve as a cooling agent for the vapor, reducing its temperature.

The authors in the same research discussed numerous advantages of the HACHP over VCHP, such as a larger temperature glide, a higher temperature lift and an enhanced capacity control. Figure 2.3 outlines that lower pressure levels can be reached with a HACHP compared to a VCHP while operating at the same temperature. The constant temperatures in the condenser and in the evaporator are represented by blue dots, while the absorption and desorption processes by the red arrows. The temperature distribution for the HACHP is not constant, but there is a temperature glide during heat transfer. This effect, named the Lorenz effect, increases the efficiency of the heat transfer when the temperature glide of the working mixture matches the temperature glide of the secondary fluid.

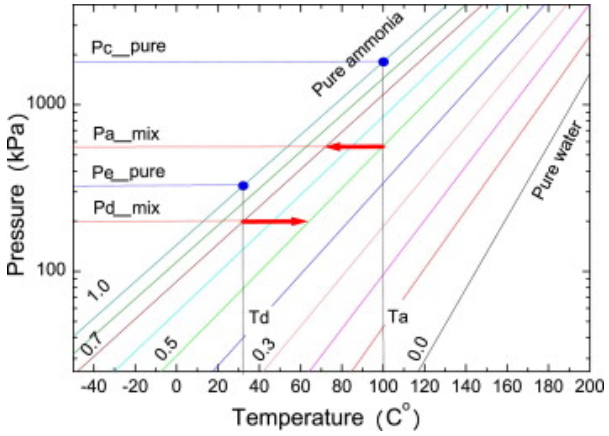

Figure 2.3: Pressure levels for hybrid heat pump cycle working with NH_3-H_2O and conventional vapor-compression cycle using pure ammonia. Figure from Kim et al. (2013).

Jung et al. (2018) also discussed how the major shortcomings of VCHPs can be overcome by HACHP applications. In their study of upgrading low waste heat streams to higher temperatures with HACHPs, the following drawbacks regarding VCHPs are mentioned:

- The use of environmentally harming fluids such as CFC, HCFC and HFC.
- The limitation on achievable temperature rise, resulting in very high pressures, which decreases the efficiency of the system and causes technical problems.
- The short range of heat source temperatures, which cannot be higher or lower than the design point due to fluctuations in the system efficiency.

In Table 5.1 a summary of the researches discussed in this section is provided.

Table 2.1: Summary of researches on HACHPs and VCHPs.

Reference	System	Highlights
Ziegler and Riesch, 1993	CRHP	• Major advantage for the CRHP is the non-constant temperature phase transition. • Higher temperatures achievable at lower pressures than with the VCHP.
Brunin et al., 1997	VCHP (hydrofluorocarbons) and CRHP (NH_3-H_2O)	• NH_3-H_2O can cover higher temperature applications with negligible emissions.
Kim et al., 2013	HACHP with additional desuperheater and rectifier	• Higher efficiency for HACHP over VCHP due to temperature glide during heat transfer. • NH_3 concentration affects the system performance.
Jensen et al., 2015	VCHP (R717) and HACHP (NH_3-H_2O)	• With the HACHP both higher temperature supply and higher temperature lifts can be obtained, extending the range of operating conditions.
Jung et al., 2018	HACHP(NH_3-H_2O)	• VCHPs mostly work with enviromentally harming fluids. • VCHPs cannot reach high temperatures due to damage for the compressor.

2.2.2. Wet compression compared to dry compression

In the previous section, it was established that CRHPs are the solution with the highest potential to upgrade waste heat streams to higher temperatures in industrial processes. Even though Jensen et al. (2015) stated that these heat pumps are theoretically able to reach very high temperatures up to 150°C, practically, researchers could not exceed temperatures over 90°C [Jung et al. (2018), Markmann et al. (2019)]. The hot temperature supply is limited by the maximum discharge temperature which the compressor can tolerate. The process of compression from low to high pressure is not an ideal process as some irreversibility occurs leading to a much higher compression discharge temperature. The extent of this inefficiency can be quantified using the isentropic efficiency, which can be defined as the ratio between the ideal work without variation in entropy $(\dot{m}(h_{2is} - h_1))$ and the specific real work $(\dot{m}(h_2 - h_1))$.

$$\eta_{is} = \frac{\dot{m}(h_{2s} - h_1)}{\dot{m}(h_2 - h_1)} \tag{2.3}$$

Hence, some researchers focused their study on a solution to reduce the compressor high discharge temperature of the HACHP while maintaining a good level of efficiency.

Kim et al. (2013), whose research was introduced in the previous section, suggested to split the compression in two stages placing an intercooler between them. However, the limit for the compressor discharge temperature was still set at 120°C to prevent oil from carbonizing. A maximum temperature supply of 90°C was reached.

Ayou (2022) used this technology in a double-lift NH_3-H_2O HACHP for simultaneous process heating and refrigerating in the food and beverage industry. In this case, two dry compression stages are implemented due to the large temperature lift for operating simultaneously with low and high temper-

atures. The system, consisting of a VCHP, for refrigeration applications, and a double stage HACHP, is able to produce hot water at temperatures between 133°C and 146°C, while chilled fluid is provided between -10°C and 10°C for process cooling.

Gao et al. (2020) proposed a similar technique. With the intention of reducing the suction temperature of the compressor, and thereby the discharge temperature, a two-stage rectification was implemented in two HACHPs coupled to each other through a subcooler. With this solution high supply temperatures (up to 120°C) and high COPs are obtained. Although both solutions achieved good results, the proliferation of this type of heat pump is still blocked due to the complexity of the system and high investment costs.

Another solution to decrease the compressor discharge temperature consist in injecting liquid in the compression process. In this way, the liquid can act as lubricant substituting the oil and decreasing the vapor temperature. In Figure 2.4, the T-s diagram displays two possible solutions. The red line on the diagram represents the process of isentropic compression.

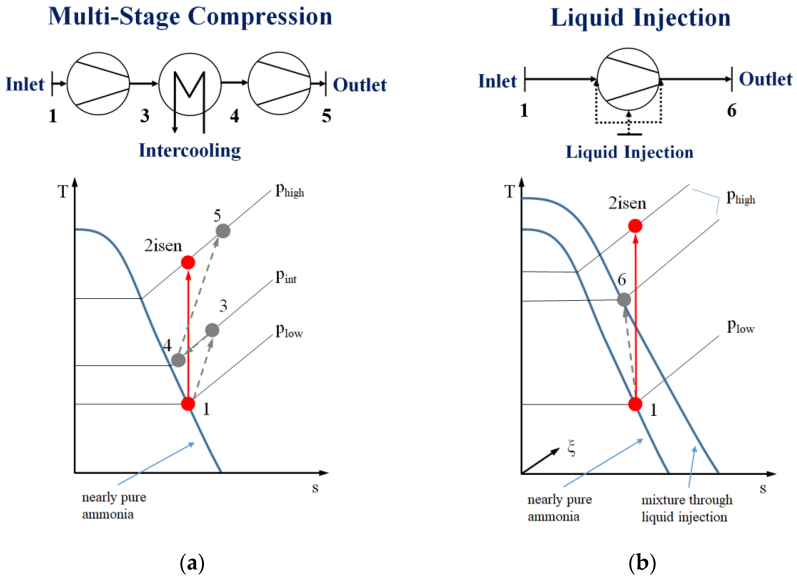

Figure 2.4: Two potential compression solutions shown in the T-s diagram. (a) Two-stage compression with an intercooler. (b) Single-stage compression with liquid injection. Figure from Ahrens et al. (2021).

A significant amount of research has been conducted on the positive and negative effects of wet compression compared to dry compression and it will be discussed in this section.

Van de Bor et al. (2015) discussed the energetic and economic advantages of different types of technologies which are used as heat recovery systems for waste heat temperature of 45–60 °C from industrial processes, since a significant quantity of waste streams is rejected into the environment at these temperatures. CRHPs have been identified as the best technology to achieve high temperatures and high temperature lifts since they combine the advantages of an absorption heat pump (using fluids with non-isothermal phase transitions) and a vapor-compression heat pump. However, a distinction is made between CRHPs operating under dry and wet compression conditions.

- Dry compression enables the highest maximum attainable temperature as there is a larger enthalpy variation in the resorber due to superheating. For wet compression, temperature lifts up to 150°C are possible.
- For dry compression, high temperatures may lead to degradation of the refrigerant and technical instabilities of lubricating oil. For wet compression, oil is not required as the compressor is lubricated by the liquid itself.
- For dry compression, accumulation of oil can be found at the heat exchanger surface, leading to a performance degradation. An increase of up to 50% in COP can be observed if wet compression is applied instead of dry compression.

- CRHPs show the best economical advantages since they can use the full temperature glides on both heat exchangers. When wet compression is applied, the discharge temperature of the compressor is reduced, the efficiency is improved and therefore the economic performance is enhanced.

Similarly, Itard (1998) listed the advantages and disadvantages when wet compression is applied for different types of refrigerants. Among others, she investigated pure refrigerants, such as R12, and mixtures, such as NH_3-H_2O. The conclusion of this study was that wet compression is not always advantageous for pure refrigerants. However, for some of them, there is a clear benefit when high temperatures are being targeted. With wet compression, the superheating zone would be avoided, ensuring mechanical stability of the compressor and thermo-chemical stability of the refrigerant and the oil. For non-azeotropic mixtures wet compression becomes very interesting since it can lead to a higher COP and lower discharge temperatures. However, these advantages can vanish whenever wet compression is not properly achieved in the compressor or when isentropic losses are too high. Hence, the importance of using optimal conditions during wet compression operations is very clear.

In addition to NH_3-H_2O, Gudjonsdottir and Infante Ferreira (2020) studied the impact of adding CO_2 to the mixture. In this work, they examined the thermodynamic and economic performance of a compression-resorption heat pump operating with NH_3-H_2O or NH_3-H_2O-CO_2 in two different industrial scenarios. In the first scenario the waste heat stream is upgraded from 90°C to 130°C, with a temperature glide in the resorber of 40 K, while in the second scenario the stream is heated from 60°C to 140°C, with a larger temperature glide in the resorber (80 K). The following conclusions were drawn for the two scenarios:

- In the first scenario, results show that a lower vapor quality leads to a higher isentropic efficiency and, therefore, a higher COP (Figure 2.5a). The thermodynamic optimum occurs at low NH_3 concentrations. In contrast, the economic optimum is found at high NH_3 concentrations, since a higher NH_3 concentration results in a higher density of the mixture causing the required compressor power to decrease. When 5% CO_2 is added, the isentropic efficiency and COP improve.
- In the second scenario, adding CO_2 leads to a lower temperature glide of the mixture, while the temperature glide of the resorber is high (80 K), reducing the COP. For low vapor qualities, the temperature glide in the mixture decreases as well, leading to a lower COP (Figure 2.5b). The trend for the economic optimum aligns with the first scenario: the payback period decreases for higher ammonia concentrations and lower vapor qualities.

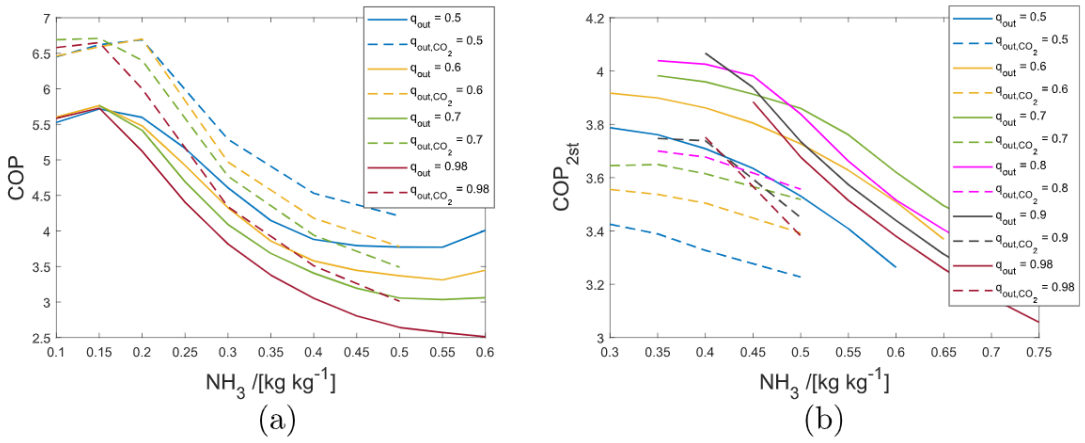

Figure 2.5: COP as a function of the NH3 concentration for various compressor outlet vapor qualities when a waste heat stream is heated (a) from 90 to 130 °C and (b) from 60 to 140 °C. The solid lines are the results for NH_3-H_2O and the dotted lines with added 5 wt% CO_2. Figure from Gudjonsdottir and Infante Ferreira (2020).

The payback period is an important factor to take into account when selecting a heat pump. The Gudjonsdottir and Infante Ferreira (2020) study showed that even at high temperature lifts, CRHPs have an economic advantage over other types of heat pumps. Ammonia-water is still the preferred

type of mixture for these heat pumps. Adding CO_2 only shows energetic advantages only when the temperature glide is not too large. However, the economical impact of adding CO_2 should be taken into account.

CRHPs have been identified as an ideal technology for large temperature lifts while maintaining high performance, as shown in the study of Gudjonsdottir and Infante Ferreira (2020). For the same reason, Van De Bor et al. (2014) evaluated the integration of heat pumps in distillation columns in 50 different industrial scenarios. For the purpose of this study, the isentropic efficiency of the compressor was kept at 70%. The following conclusions were drawn:

- The CRHPs show economic and energetic advantages up to temperature lifts of 124 K.
- The glide of the process should be matched by the resorber temperature glide to have the best results.
- The ideal vapor quality at the resorber inlet is 1.
- The ammonia concentration is highly dependent on the operating conditions of the resorber.

As evident from various scientific sources, the best performance, in the context of upgrading waste heat streams temperatures, is achieved when the liquid is compressed along with the vapor into the compressor. Therefore, it is advantageous to analyze wet compression.

In Table 2.2, a short summary of the researches on wet compression is provided.

Table 2.2: Summary of research studies on CRHPs employing wet compression.

Reference	Highlights
Itard, 1998	• For pure refrigerants there might be advantages in applying wet compression, for mixtures wet compression is always beneficial. • Higher COP can be achieved if isentropic losses are small.
Van De Bor et al., 2014	• CRHPs show economic and energetic advantages up to temperature lifts of 124 K. • The ideal vapor quality at the resorber inlet is 1.
Van de Bor et al., 2015	• For dry compression, the highest temperatures are attainable, however, technical instabilities due to oil in the compressor make them practically unfeasible. • Wet compression can be employed without oil, leading to better performances and lower costs.
Gudjonsdottir and Infante Ferreira, 2020	• The benefits of adding CO_2 to NH_3-H_2O depend on the application. For high temperature glides no benefits are encountered. • The thermodynamic optimum depends on the operating conditions and generally diverges from the economic optimum.

2.3. The compressor

When operating compression-resorption heat pumps, the compressor is identified as the main bottleneck according to several authors [Jensen et al. (2015), Kim et al. (2013), Brunin et al. (1997), Ahrens et al. (2023)]. Normally, both the process side and the bearings of the compressor are lubricated by oil for the following reasons:

- To reduce friction on moving parts of the compressor, avoiding corrosion and damage.
- To cool the fluid during compression.

- To seal against refrigerant gas leakages.

However, when high temperatures are reached, oil degradation can occur, resulting in several issues which can lead to a reduction of the performance and component damage. Additionally, expensive devices are needed after compression in order to carefully separate the process fluid from the oil due to the possible accumulation of oil on the surface of the heat exchangers.

As mentioned by Jensen et al. (2015), the use of an oil-free compressor might relax the limit on the compressor discharge temperature, allowing the supply of high temperatures up to 150°C. If well separated from the process side the bearings could still be lubricated with oil which will not interfere with the working fluid. However, an alternative solution needs to be found for lubricating the process side of the compressor against leakage and damage of the component itself. Employing wet compression, the liquid refrigerant can function as lubricant in the process side. As such, both oil contamination and irreversibility caused by superheating of the vapor can be avoided, enhancing the performance and reducing the compressor power. In Figure 2.6, the temperature-enthalpy (T-h) diagram is plotted for a compression-resorption cycle operating under wet compression conditions (Figure 2.7a) and a vapor-compression cycle (Figure 2.7b-c). Figure 2.7a shows that under wet compression conditions, very high discharge temperatures are avoided.

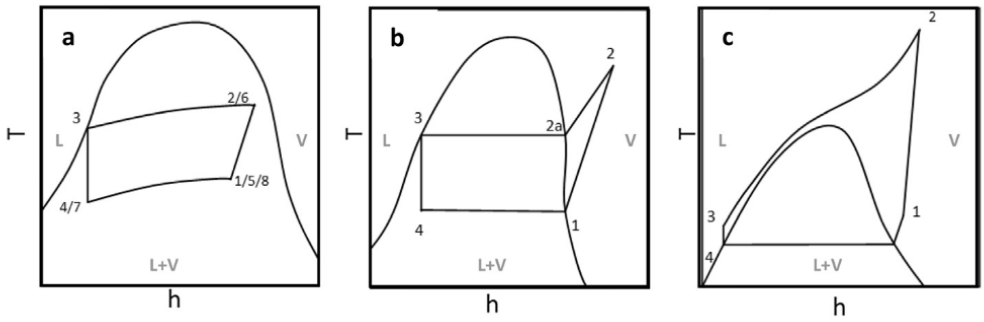

Figure 2.6: Temperature-enthalpy diagrams for (a) compression-resorption, (b) subcritical vapor-compression and (c) trans-critical vapor-compression heat pumps. Figure from Van de Bor et al. (2015).

An essential requirement for wet compression is a compressor resistant to liquid. Zaytsev (2003) selected positive displacement compressors as main candidates for wet compression, due to their ability to achieve high pressure ratios. However, among these, reciprocating compressors are not ideal since the liquid may cause severe issues due to hydraulic locking. If liquid slugging occurs, the valves of the reciprocating compressor would be seriously damaged. On the contrary, screw compressors have no valves or thin blades that can be damaged by the liquid and are therefore more suitable for operations with liquid. The twin-screw compressor is a positive displacement machine with two parallel helical rotors, named the male and female rotor (Figure 2.7). The male rotor has convex lobes and the female rotor has concave cavities causing them to mesh into each other.

Figure 2.7: Twin-screw compressor with timing gears. Courtesy of Atlas Copco. Figure from D.L.Thurrott (2022).

Wet compression in twin-screw compressors can be carried out either with or without liquid injection of the refrigerant. In the first scenario, a small part of the liquid refrigerant is withdrawn during compression and returned to the suction side. In the second case, no injection is performed and the entire flow is compressed where-upon it fully enters into the resorber.

After identifying a suitable type of compressor, Zaytsev (2003) collected and analyzed experimental data of a modified twin-screw compressor operating with NH_3-H_2O under wet compression conditions with liquid injection. During his study, Zaytsev (2003) claimed that liquid flow in the compressor can have both a positive and negative influence on the COP. On the upside, it seals the leakage paths for the vapor, it lubricates the process side of the compressor and it cools down the flow. However, there can be leakage flows, which evaporate and which can cause irreversible losses when going from the high pressure to low pressure zones. The performance of the overall heat pump strongly depends on the efficiency of the compressor, which in turn depends on the operating conditions. Hence, it is essential to investigate the specific operating conditions that maximize the compressor's efficiency in that specific case.

According to Zaytsev (2003), Infante Ferreira et al. (2006) and Ahrens et al. (2023), liquid injection is a good solution to decrease the compressor discharge temperature and improve the efficiency. Nonetheless, some complications arise when the extracted liquid flashes and thus generate more vapor, when going from the high pressure to the low pressure zone. This additional amount of vapor needs to be recompressed, which increases the compression power.

Other researches, such as Gudjonsdottir et al. (2019), suggested to employ wet compression without liquid injection. For this study, the model of Zaytsev (2003) was modified removing liquid injection. Gudjonsdottir et al. (2019) investigated twelve different scenarios by varying the ammonia concentration, the compressor speed and the outlet vapor quality. Results showed that:

- If the compressor speed is increased, the flow rate through the compressor increases leading to a larger entropy production. However, this can also be beneficial because it leads to a larger displacement of working fluid. Generally, the compressor should operate with a minimum speed of 10000 rpm.
- The optimal ammonia concentration depends on the desired supply temperature. Even if for higher ammonia concentrations higher efficiencies are achieved, the entropy production is similar for the three concentration levels. For most industrial applications ammonia concentration varies between 20% and 40%.
- Theoretically, the optimal outlet vapor quality is close to unity. Practically, this should be avoided due to the risk of superheating the vapor. In that case, a higher discharge temperature and a lower isentropic efficiency would be obtained. On the contrary, if the vapor quality is too low, a high amount of liquid in the compressor may lead to hydraulic locking. The compressor outlet vapor quality should be maintained in a range between 50-70%.

The work on the experimental setup used by Gudjonsdottir was used as a basis for the study by Kothari (2020), who investigated the operating conditions for which a high value of isentropic efficiency is obtained. Parameters, such as inlet vapor quality at the compressor, compressor speed and ammonia concentrations, have been varied using a homogeneous thermodynamic model. The following conclusions can be drawn when the inlet vapor quality at the compressor is increased:

- A lower isentropic efficiency is obtained due to the smaller amount of liquid in the compressor. This happens because the liquid has the ability to seal the leakage paths for the gas and to lubricate the compressor.
- A higher volumetric efficiency is obtained.
- A lower temperature lift is obtained. A higher inlet vapor quality leads to lower pressure ratios in the compression process.

Using the homogeneous approach the highest experimentally obtained value of isentropic efficiency was 0.44. In some cases, the vapor at the discharge port of the compressor was found to be superheated. However, the high discharge temperature was disguised by the low temperature measured by

the sensor, which probably only detected the liquid temperature. This possibility leads to the conclusion that a heterogenous model, in which the liquid and vapor are treated separately, would be most applicable. In addition, there are high discrepancies between the results of the model and the experimental data, suggesting that the model is not accurate, probably because the liquid and the vapor phase are not in equilibrium.

In Table 2.3, the conclusions of the discussed research are highlighted.

Table 2.3: Summary of researches on the compressor used for wet compression.

Reference	Highlights
Zaytsev, 2003	• COP depends on the isentropic efficiency. • Liquid in the compressor has both positive and negative effects: beneficial for lubrication, cooling and reducing leakages. Injection of liquid is critical because it could also increase the compression power.
Gudjonsdottir et al., 2019	• The optimal NH_3 concentration depends on the temperature application. • Outlet vapor quality needs to be maintained between 0.5-0.7. • Lower vapor quality implies minor irreversibility.
Kothari, 2020	• When increasing the inlet vapor quality the isentropic efficiency decreases. The liquid seals the leakage paths for the gas. • When increasing the inlet vapor quality the volumetric efficiency increases. • When increasing the inlet vapor quality a lower lift is obtained. Lower pressure ratios are obtained as well.

3

Research question

The objective of the research thesis is:

To explore the operating parameters at the compressor inlet while working with an NH_3-H_2O mixture under non-equilibrium conditions, aiming to maximize compressor efficiency and achieve elevated sink temperatures (≥120°C).

The quest to fill the void in the market of heat pumps reaching temperature levels between 120-140 °C with relatively low cost and high efficiency has been the focus of research in this field for the last two decades. Vapor-compression heat pumps have been excluded because of their limited single-stage temperature lift and high pressure levels. Higher temperatures can be achieved using multiple stages at the expense of both energetic and economic performance. Compression-resorption heat pumps can offer a good solution for their ability to operate using a mixture with non-isothermal phase transition and low environmental impact. Compression-resorption heat pumps can operate with wet compression or dry compression:

- For wet compression both vapor and liquid are compressed, the superheating of the vapor can be avoided or reduced. For dry compression only the vapor is compressed, reaching high discharge temperatures. This leads to higher losses, lower efficiency and thermal instabilities of the oil.
- For wet compression the liquid itself can be used as lubricant. For dry compression the oil is fundamental for lubricating the compressor. The oil can agglomerate on the surface of the heat exchangers, reducing the heat transfer performance and increasing the maintenance costs.
- For wet compression, theoretically, lower investment costs are needed. For dry compression, a separator, an additional heat exchanger and a pump lead to higher investment costs.
- Wet compression is still under development. A compressor able to operate with liquid and vapor, keeping a good level of performance, is required on the market. Dry compression is widely applied.

The research on CRHPs operating with wet compression suggests their ability to reach high supply temperatures and high temperature lifts with a relatively high efficiency, potentially causing a paradigm shift in heat pump technology. The missing ingredient for this technology is a component able to compress a vapor-liquid mixture with a good value of isentropic efficiency. The absence of such commercially viable technological solution inhibits the proliferation of CRHPs in industrial processes. The void in the market and the need to recover waste heat lead this study to investigate the operating conditions in which a compression-resorption heat pump can deliver high temperatures (≥120 °C) with an acceptable value of isentropic efficiency for the compressor. Based on the literature, the following challenges need to be addressed:

- **Optimization of the compressor for oil-free operations:** Liquid refrigerants can replace the oil for lubricating the compressor. Liquid injection is beneficial in lowering the vapor temperature, however, it also affects the efficiency because some vapor must be recompressed.

- **Selecting the relevant model between homogeneous or heterogeneous:** The actual mechanism behind wet compression remains unclear. The liquid might be in equilibrium with the vapor during compression (homogeneous approach) or might have different properties (heterogeneous approach). According to the chosen approach, the output conditions will be different.
- **Reduction of the compressor discharge temperature:** Achieving high supply temperatures is a particular challenge due to the rise of multiple issues which can be related to high discharge temperatures after compression (oil degradation, compression power increase and material damage). As suggested by Van De Bor et al. (2014), the working fluid at the compressor discharge should be saturated vapor.
- **Minimization of leakages during compression:** As discussed by Zaytsev (2003), leakages occur during compression across cavities within the compressor. The rotational angle and the position of the sealing lines between sequential cavities are relevant for the minimization of these leakages. Modelling and testing the limitation of the back flow from the gap seal could show considerable effects on the compressor performance.

With the objective of investigating the operating conditions for wet compression, a numerical model is developed during this research thesis. The model reproduces the compression of ammonia-water mixture under a heterogenous approach without liquid injection. Differently from other models, the liquid and the vapor are not at equilibrium during compression. Both phases show different temperatures, concentrations, densities, however, the pressure in the cavity is uniform. This will lead to a better understanding of the behavior and interaction between the liquid and the vapor phase. In this case, heat and mass transfer between the vapor and the liquid cannot be neglected. This research study investigates the influence of the flow from the gap seal on the compressor's operating conditions.

4

Experimental setup

An experimental setup of a compression-resorption heat pump has been built in the Process & Energy Lab at Delft University of Technology. The primary focus of the CRHP setup is the oil-free twin-screw compressor provided by Atlas Copco, market leader in air compressors. The planned experimental objective involved conducting experiments in which the compressor would operate with the refrigerant in both liquid and vapor phases, with the intention of varying input parameters such as temperature, ammonia concentration, pressure, and vapor quality of the mixture. With this intention, the common configuration of the heat pump was modified. In the present case, the desorber is replaced by a vapor and a liquid line, in order to be able to control the vapor quality and the temperature at the inlet of the compressor. In Figure 4.1, the P&ID diagram of the experimental setup is shown. The double phase

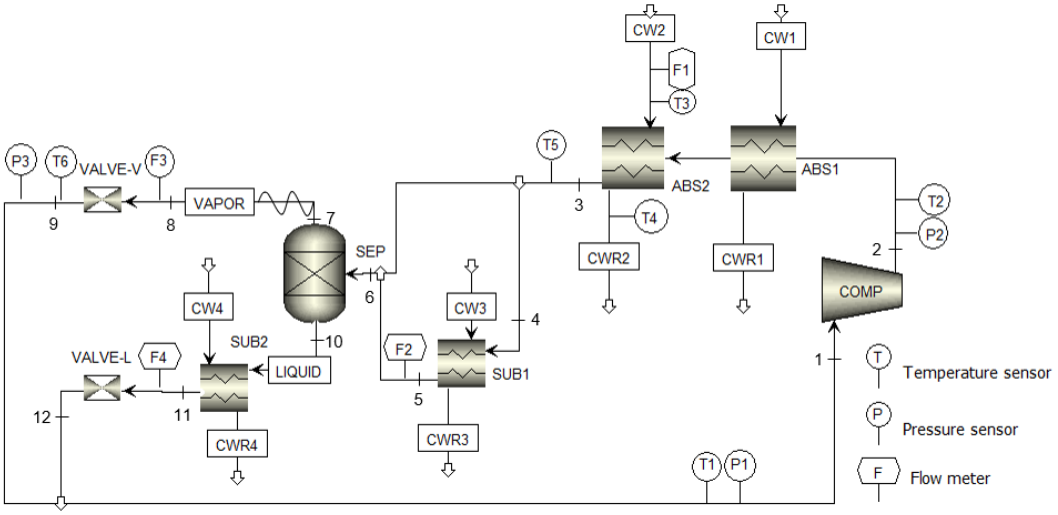

Figure 4.1: Simplified P&ID diagram of the experimental setup.

flow is compressed with the oil-free twin-screw compressor (1→2). To monitor the flow, pressure and temperature sensors are positioned at both the compressor's inlet and outlet. The compressed flow then passes through absorbers, which consist of two plate heat exchangers connected in series (2→3). Two separate cooling water flows are used as secondary fluid. After absorption, a part of the main flow is withdrawn in order to measure the ammonia concentration at this point. For this purpose, the by-pass of the main flow is subcooled (4→5) before entering the Coriolis density measurement (F2), as this device cannot handle temperatures which are too high. Subsequently, the total flow is split in a separator into a vapor and liquid flow in order to vary the operating conditions at the inlet of the compressor. The vapor is slightly superheated through an electric tracing system (7→8) , while the liquid is brought into a subcooled state using a subcooler (10→11). Both flows are expanded to the low pressure level of the system through expansion valves. A fraction of liquid might flash, increasing the vapor stream. The two

flows are rejoined at the inlet of the compressor, where the liquid is sprayed through a spray nozzle. It is highly possible that in this phase the vapor and the liquid are in equilibrium. The inlet conditions of the compressor, specifically the temperature and pressure, are measured through sensors before entering in the compressor. The vapor-liquid flow is then compressed again, starting a new cycle.

4.1. Recommissioning of the experimental setup

The experimental setup was decommissioned in 2020. During this time the setup has been completely disassembled and transported for maintenance activities in the lab. Because of this, every connection has been unscrewed and some components have been damaged. Before running again, it is necessary to recommission the experimental setup.

Leakages in an experimental setup can have negative consequences as they affect the accuracy of data and pose safety hazards, especially within the scope of this thesis where the CRHP operates with ammonia, an hazardous fluid. According to the extent of exposure, ammonia can cause severe injuries and burns. In addition, it is also explosive and flammable. Hence, it is essential to perform leak detection before performing experiments.

Due to the complexity of the setup, the first four months of this study were dedicated to make the setup operational again. During this time a thorough leak detection has been conducted. Several connection points were leaking, a weak torque was applied to the flanges and an unused experimental setup was connected to the considered one. Despite separating the two systems using valves, concerns arose about the condition of these valves, which pose a potential risk to the reliability of the experimental data. Consequently, both systems were disconnected as a precautionary measure. The leakages were identified performing pressure drop tests. The pressure was monitored in four different parts of the CRHP using pressure meters, which are positioned at the inlet and at the outlet of the compressor, in the vapor line and in the liquid line. The vapor and liquid line are shown in Figure 4.2.

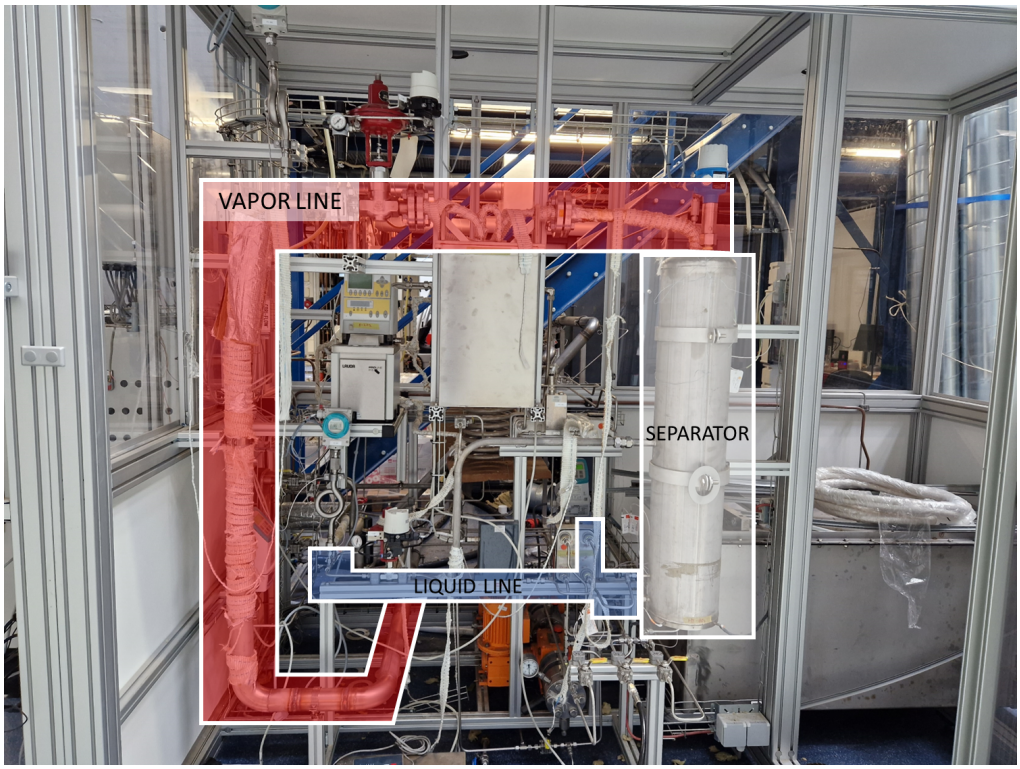

Figure 4.2: Part of the experimental setup. In the picture: the separator, the vapor line and the liquid line.

The setup was pressurized with nitrogen at different pressure levels, progressively from 3 bar to 13 bar. During the leakage detection the working assembly was isolated into four different sections using valves. This strategic isolation allowed for a more precise identification of any potential leakage. It was

essential to replace damaged components, e.g. a ball valve used for disconnecting the discharge line from the compressor side. The assembly consists of ten flanges, which were individually inspected for leakages. Different torques were applied until the flanges were completely leak tight. Among them, two flanges appeared to be damaged. As a consequence they were removed and replaced with two different pipelines: the discharge line and the vapor line. In addition, the pipeline containing liquid flow had to be reinstalled again since it was missing from the setup. While it was possible to identify all the leakages in the discharge line, in the vapor line and in the liquid line, a pressure drop was still observed at the compressor side. All the flanges in proximity of the compressor were identified to be leak tight. It is reasonable that the fluid leaks through the clearances between the moving parts of the compressor, which are filled with fluid during compression. During the recommissioning of the setup other basic, but essential activities took place. Since high temperatures (up to 140°C) were intended to be reached, a proper insulation is key. The proper materials and the respective geometry to better insulate the setup were investigated.

4.2. Modification of the experimental setup

The experimental results obtained in 2020 provide the input parameters at the inlet of the compressor for the vapor and the liquid flow. However, these are not the final conditions at the compressor suction. The flow that comes from the gap seal has a large impact on both the compressor input conditions and its performance. The flow from the gap seal probably consists of vapor and has the same concentration of the vapor flow at the compressor discharge. This significantly increases the temperature at the compressor suction, pushes the ammonia concentration of the mixture to higher values and impacts the suction mass flow rate. In the previous experiments, this flow was uncontrolled and its impact could not be quantified. Hence, during this work, the compressor side was modified introducing a valve and a pressure gauge on the line from the gap seal to suction, in order to quantify and control the flow. The pressure gauge is required to estimate the mass flow rate of the valve with the isentropic nozzle flow model, which will be discussed in chapter 5. Knowing the downstream pressure and the upstream pressure, the mass flow rate can be derived from the pressure difference. Figure 4.3 shows the location of the gap seal line, of the pressure gauge and of the valve.

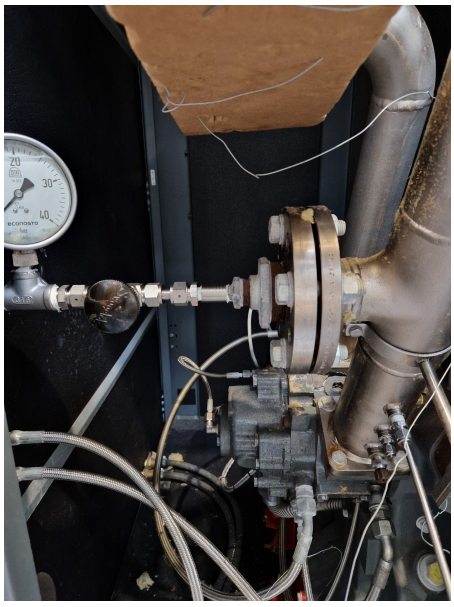

Figure 4.3: Valve on the return line from the gap seal.

Even though the experimental setup is now ready to be running again, experiments were not performed during this research thesis. Some setbacks, such as contractor issues, lack of communication by the industrial partner and the absence of SOPs at the P&E lab, significantly delayed the start of the experiments.

5

Numerical modelling

In order to investigate the best operating parameters to apply for wet compression, the twin-screw compressor operation was digitally recreated in MATLAB. In this way, thermodynamic properties, such as suction pressure, suction temperature, pressure ratio, inlet vapor quality or ammonia concentration, can be varied to study the effect they have on the compressor's efficiency and on the discharge temperature of the fluid. The finite volume method has been employed to simulate the dynamic evolution of fluid properties during the compression process. The thermodynamic properties are obtained through REFPROP [Lemmon et al. (2018)] and XNH3H2O [Rattner (2017)]. The *compressor model* is based on the following assumptions:

- The liquid and vapor phase are homogeneous at the suction. Once compression starts, they behave heterogeneously. The liquid and the vapor phase have different properties (temperature, concentration, density), however, the pressure is uniform through the compression cavity.
- The liquid is pushed against the compressor walls due to centrifugal forces, creating a net separation between the thin film of liquid and the vapor bulk.
- Heat transfer between the working fluid and the compressor casing is considered negligible.
- Mechanical losses are taken into account by introducing the mechanical efficiency obtained from the experiments.

Heat transfer between the compressor casing and the working medium was calculated for different data sets considering the temperature distribution across the length of the rotor. In each data set the heat transfer was negligible (about 2% of the compression power). Ahrens et al. (2019) investigated the heat losses to the environment during the compression process. Even when applying the highest heat transfer coefficient, the influence of the heat losses on the compression process is minimal. Even if the fluid temperature significantly increases during compression - thus creating a large temperature difference between the fluid and the environment - the cavity volume, and therefore the available heat transfer area, considerably decreases. Mechanical losses are caused by friction between the rotors, in the seal and in the bearings. These have an impact on the isentropic efficiency and on the lifetime of the compressor parts. They can usually be estimated using data charts supplied by the manufacturers. Due to the unavailability of these data, the mechanical efficiency values derived by the experimental data are used as approximations for these losses. The mechanical efficiency also includes losses generated by the friction between the working medium and the mechanical parts.

For clarity, three different compressors are used in this work:

- The experimental compressor: the compressor used in the setup at P&E lab.
- The reference compressor: the compressor similar to the examined prototype disassembled for measurement (not used in the setup).
- The digital compressor: the compressor designed in MATLAB as combination of the two compressors.

5.1. Geometrical features

The numerical computation requires the knowledge of the geometry of the compressor. In this section, the computation of the different port areas and leakage paths are explained in detail. Few geometrical features of the experimental compressor are known and they are listed in Table 5.1.

Table 5.1: Geometrical features of the experimental compressor.

Maximum volume per cavity (V_{max})	5.72 10^{-5}	m^3
Male rotor diameter (D_m)	0.084	m
Length of the rotor (L)	0.084	m
Number of lobes on male rotor (z_1)	4	
Number of lobes on female rotor (z_2)	6	
Clearances size (C)	0.05	mm

Since several information necessary for the computation of the geometrical curves are missing, the geometrical model is based on the work of Zaytsev (2003) and Tang (1995). The two researches recreated the curves of the compressor cavity volume, of the suction and discharge port areas and the leakage paths as a function of the male rotor angle. These curves are based on a compressor with geometrical features different from the experimental compressor. Due to the large difference in size of the compressors, the curves from the work of Zaytsev and Tang were adapted to the reference compressor, which has geometrical features similar to the experimental compressor, such as the length of the rotor. The diameters of the rotors of the reference compressor are slightly smaller. Kothari (2020) measured the compressor port locations for the female rotor lobe of the reference compressor. Due to the fact that Zaytsev (2003) developed the geometrical curves with respect to the male rotor lobe, the locations were converted as a function of the male rotor lobe with the following relation:

$$\frac{\phi_2}{\phi_1} = \frac{z_1}{z_2} \tag{5.1}$$

5.1.1. Cavity volume

The cavity volume in a twin-screw compressor is generated by the interaction of the female and male rotors, both of which have a helical profile and rotate in opposite directions. Consequently, the lobes of the male rotor interlock with the cavities formed between the lobes of the female rotor, resulting in a series of cavities. The development of one cavity is represented in Figure 5.1. The cavity progressively

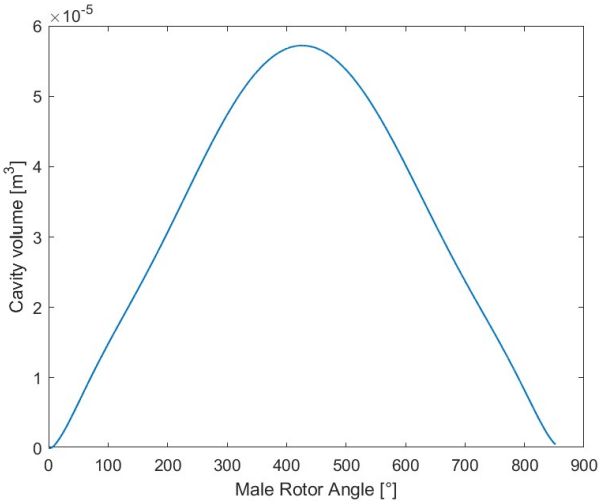

Figure 5.1: Evolution of the volume cavity as a function of the male rotor angle.

grows from 0 to the maximum value. Throughout this process, the cavity remains in contact with the suction port, facilitating the flow from the suction side. After the maximum volume is reached, the volume decreases back to zero; in doing so the fluid trapped inside the cavity is compressed. When

the discharge port opens, the compressed fluid flows out until the cavity volume becomes zero again. Since the maximum volume cavity is known, the volume curve was reproduced accounting only for its maximum and the relation with the male rotor angle. The maximum is reached after the male rotor turns 426°, corresponding to a rotation of 284° of the female rotor. A complete compression process (suction, compression and discharge) involves a rotation of 852° of the male rotor.

5.1.2. Suction phase

The fluid enters during the suction phase through the suction ports. These suction ports are expressed as a function of the male rotor angle. The opening and closing of the suction ports have a large influence on the mass flow rate of the compressor and thus on the performance. The suction phase was measured with respect to the female rotor and converted as a function of the male rotor (Table 5.2).

Table 5.2: Rotor angles during suction phase.

	ϕ_2	ϕ_1
Suction starts	0°	0°
Maximum volume	284°	426°
Suction ends	340°	510°

Various studies have shown that only one suction stop angle on the female rotor side exists, which can be obtained using the following equation:

$$\phi_2 = \phi_1 \frac{z_1}{z_2} + \frac{360°}{z_2} \tag{5.2}$$

For the considered compressor, the ideal closing male rotor angle for the suction port would be 420°, corresponding to the angle for which the volume is at its maximum. Since the suction port closes later than the ideal position, some mass could flow out, reducing the efficiency. The theoretical shape of the suction port was computed by Tang (1995) and Zaytsev (2003). As mentioned before, the compressors used in the two studies are larger than the experimental and reference compressor. For this reason, the shape of the ports was recreated, but the dimensions were adjusted according to the reference compressor. Figure 5.2a and Figure 5.2b show the axial and the radial suction port, respectively.

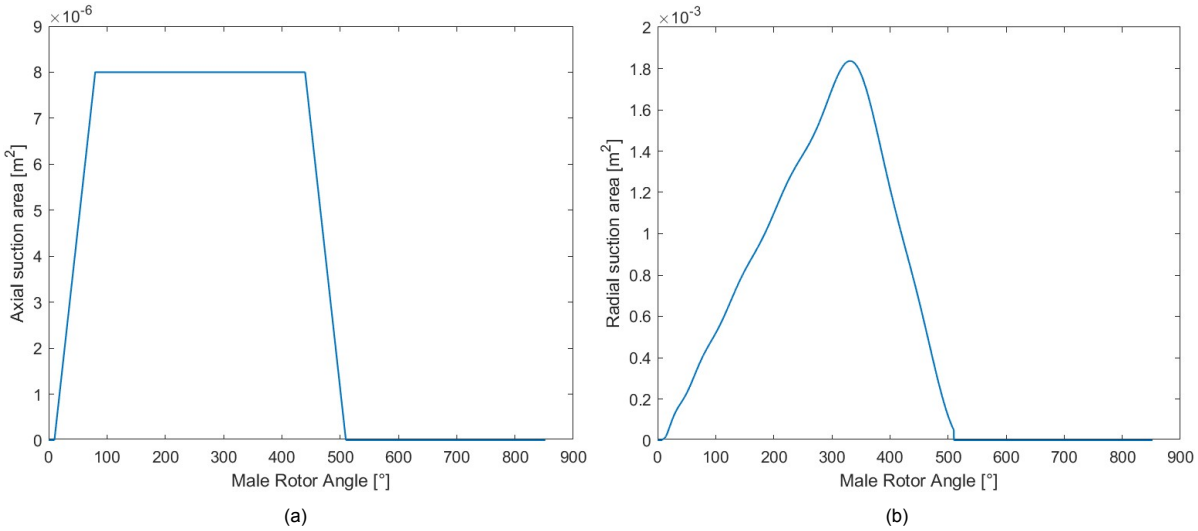

Figure 5.2: (a) Evolution of the axial suction area and (b) evolution of the radial suction area as a function of the male rotor angle.

5.1.3. Discharge phase

The reference and experimental compressor only have one axial discharge port, while no radial discharge port is present. The discharge port size was measured for the reference compressor. The axial

discharge port is shown in Figure 5.3. Similar to the other ports, the opening and closing times were measured with respect to the female rotor and converted with respect to the male rotor (Table 5.3).

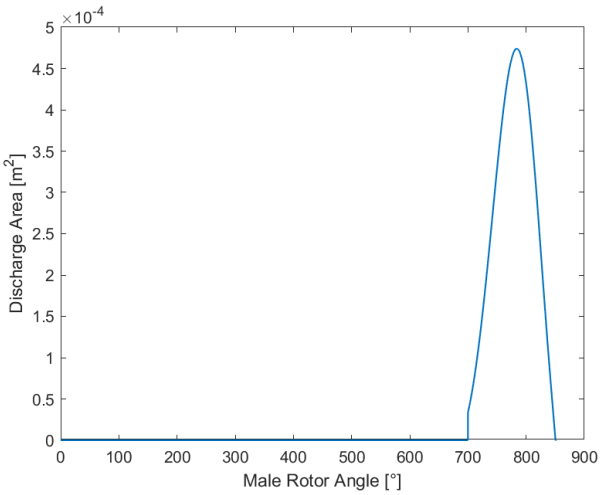

Figure 5.3: Evolution of the axial discharge area as a function of the male rotor angle.

Table 5.3: Rotor angles during discharge phase.

	ϕ_2	ϕ_1
Discharge starts	478°	717°
Discharge ends	568°	852°

5.1.4. Leakage paths

In a twin-screw compressor, it is necessary to have a small gap between the moving parts to account for machining tolerance, force deflection and thermal expansion. However, the pressure difference through these clearances can cause leakages in different parts of the compressor. The leakages impact the mass flow rate and thus the performance of the operation [Chamoun et al. (2013)]. The main leakage paths in a twin-screw compressor have been identified by Tang (1995) and are the following:

- Leakage through the contact line between rotors.
- Leakage through the sealing lines between the rotor tips of the female or male rotor and the housing bores.
- Leakage through the compression start blow hole.
- Leakage through the cusp blow hole.
- Leakage through the clearance between the end plate and the rotor end face at the suction end.
- Leakage through the clearance between the end plate and the rotor end face at the discharge end.

The cross-sectional area of the leakage paths is calculated using the following formula:

$$A = LC \tag{5.3}$$

where C is an average clearance and L is the length of the leakage path.

Figure 5.4 gives a brief overview of the direction of the different leakage flows.

The contact line between rotors is the most impacting leakage. The flow leaks across this path from the considered cavity to the suction cavity. In large compressors, the fluid may also leak from the high

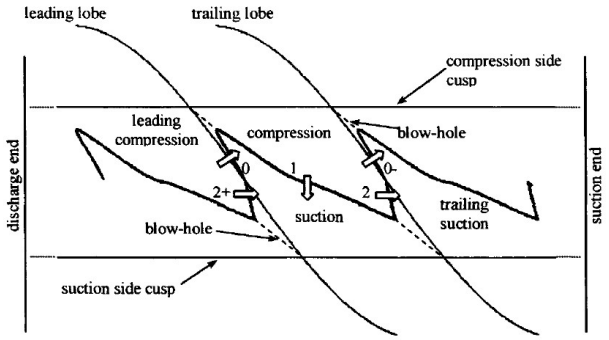

Figure 5.4: Rotors contact line with direction of leakage flows. Figure from Zaytsev (2003).

pressure side to the considered cavity or from the high pressure side to the suction cavity. However, since this compressor, in comparison with other compressors, is small, this type of leakages was not considered in this study. The contact line length of the compressor is shown in Figure 5.5.

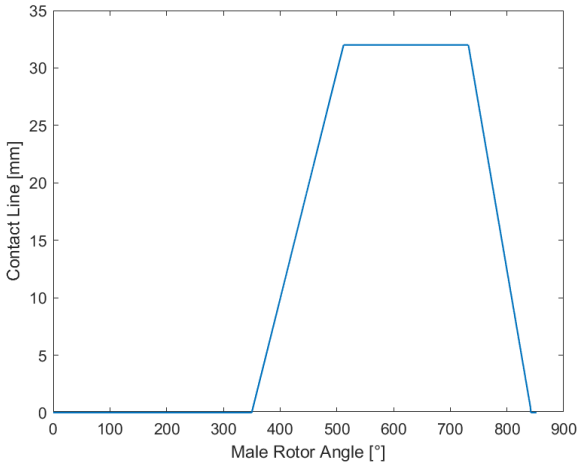

Figure 5.5: Evolution of the contact line length as a function of the male rotor angle.

A compressor's cavity is bound by four sealing screw lines between the rotor tips and the housing: male and female rotor leading tip lines and male and female rotor trailing tip lines. These sealing lines, together with the direction of leakage flows, are shown in Figure 5.6 [Zaytsev (2003)]. In Figure 5.7 the

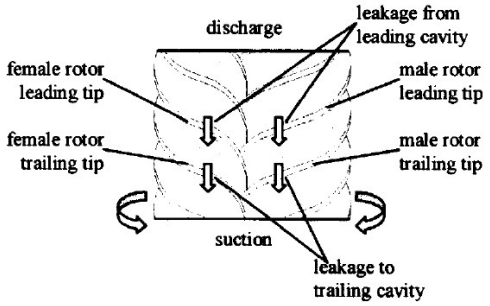

Figure 5.6: Rotor tip sealing lines. Figure from Zaytsev (2003).

leading male and female rotor tip sealing lines for this compressor are shown. The trailing line lengths are the same with a phase delay of $\frac{2\pi}{z_1}$. The maximum leakage occurs around 420°, when the cavity volume is maximum. When the volume decreases, the sealing line length decreases too. The working

fluid across the rotor tip sealing line leaks from the considered cavity to the following cavity or suction side. It may also leak from the leading cavity to the considered cavity.

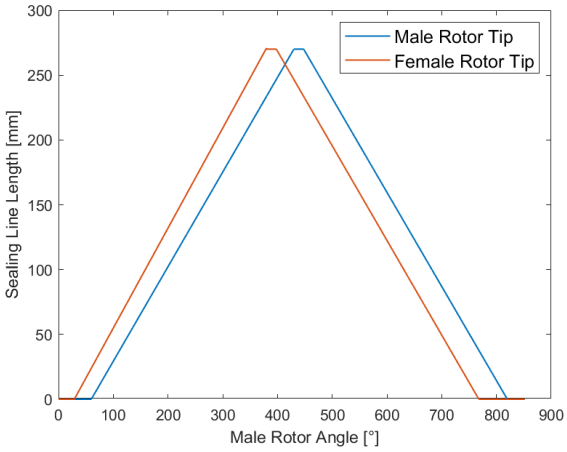

Figure 5.7: Evolution of the female and male rotor tip sealing lines as a function of the male rotor angle.

The blow hole is formed between the tips of the male and female lobes and the cusp of the housing and it causes leakages between adjacent threads. A screw compressor has a low pressure side and a high pressure side blow hole. The blow hole in the low pressure side is called compression start blow hole, while the blow hole on the high pressure side is called housing cusp blow hole [Tang (1995)].

The low pressure side blow hole, or compression start blow hole, is exposed to suction pressure of the compressor. The leakage through the compression start blow hole occurs during the suction phase and it ends just after the compression starts [Zaytsev (2003)]. However, during suction, the neighbouring cavities exhibit small pressure drops, making this leakage path only relevant once the compression phase begins. In Figure 5.8a the compression start blow hole curve is shown.

The high pressure side blow hole, or housing cusp blow hole, connects neighbouring cavities during the entire compression process. For this reason, the housing cusp blow hole greatly affects the efficiency of the compressor. The working fluid may leak to the following cavity or suction pressure through the cusp blow hole. It may also leak to the considered cavity from the leading cavity or discharge pressure. In Figure 5.8b the housing cusp blow hole area is shown.

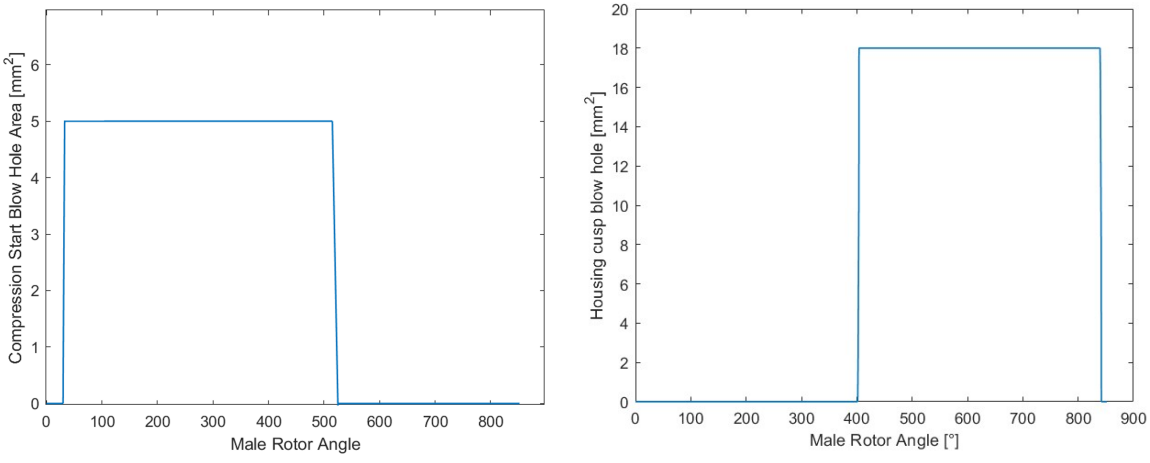

(a) (b)

Figure 5.8: (a) Evolution of the compression start blow hole area and (b) evolution of the housing cusp blow hole area as a function of the male rotor angle.

Different types of leakages occur through the end clearance. During the early stage of compression, the working fluid may leak to suction pressure across the rotor end face at the suction end. At the discharge end, two types of leakages can be distinguished. In the first type, which is shown in Figure 5.9a, the working fluid may leak from the leading cavity to the following one. In the second type, the compressed fluid leaks from the discharge chamber to the suction pressure. This leakage path is shown in Figure 5.9b.

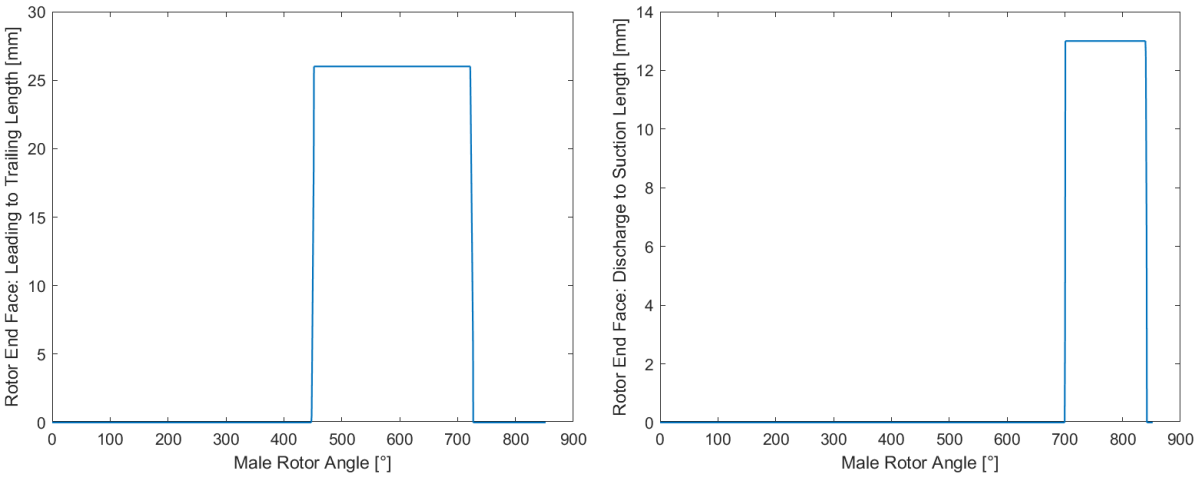

(a) (b)

Figure 5.9: (a) Evolution of the leakage path from the leading to the trailing cavity and (b) evolution of the leakage path from the discharge to the suction cavity as a function of the male rotor angle.

5.2. Thermodynamic model

The thermodynamic model is based on the work of Zaytsev (2003), which created a procedure to compute the evolution of the liquid and gas flow properties during the different phases of compression. Zaytsev (2003) followed the homogeneous approach, considering the liquid and gas to be in equilibrium during the entire compression. However, he has also proposed a different approach, where the mixture is heterogeneous, thus the liquid and gas flow are at non-equilibrium conditions. This implies that the temperature and the concentration of the ammonia in the two phases can differ from the one at equilibrium conditions at each stage. However, it is assumed that the pressure has the same value for both liquid and vapor. Since the mixture does not behave homogeneously, individual sets of governing equations need to be applied to the two phases. The governing equations are based simply on mass, species and energy balances. In addition, separate equations need to be formulated in order to evaluate the heat transfer between the two phases.

The mass conservation equations for the gas phase are described using the following formula:

$$dm_G = \sum_{k=1}^{N} dm_{G\,in,k} - \sum_{k=1}^{N} dm_{G\,out,k} + dm_{ev} \tag{5.4}$$

where m_G is for the mass of the gas phase. The subscripts indicate inflows (in), outflows (out) and mass evaporated (ev) in the considered cavity. In the case of evaporation dm_{ev} is positive, while in case of condensation dm_{ev} is negative. The conservation of energy for the gas phase can be described using the following equation:

$$\delta Q_{SG} - \delta Q_{GL} + \sum_{k=1}^{N} h_{Gin_k} dm_{Gin_k} - h_G \sum_{k=1}^{N} dm_{Gout_k} + h''_G dm_{ev} = dH_G - V_G dp \tag{5.5}$$

Here, δQ_{SG} is the heat exchanged between the compressor walls and the gas; δQ_{GL} is the heat transferred from the gas to the liquid; h_{Gin_k} is the specific enthalpy of the incoming gas from suction, discharge or leakage paths; h_G is the specific enthalpy of the gas in the considered cavity, h''_G is the specific

enthalpy of the saturated gas at liquid temperature and equilibrium concentration; V_G, H_G and p are the volume, enthalpy and pressure of the gas in the control volume. The conservation equation for the ammonia concentration is:

$$d\left(m_G X_G\right) = \sum_{k=1}^{N} X_{Gin_k} dm_{G\,in_k} - X_G \sum_{k=1}^{N} dm_{G\,out_k} + dm_{ev_{NH_3}} \tag{5.6}$$

Here, X_G is the concentration of ammonia in the gas phase, X_{Gin_k} is the concentration of ammonia in the incoming gas flow and $dm_{ev_{NH_3}}$ is the mass of ammonia evaporated. The same governing equations can be applied for the liquid phase. The conservation equation for the liquid mass can thus be described as:

$$dm_L = \sum_{k=1}^{N} dm_{L_{in,k}} - \sum_{k=1}^{N} dm_{L_{out,k}} - dm_{ev_{NH_3}} \tag{5.7}$$

The conservation of energy for the liquid phase is described with the following formula:

$$\delta Q_{SL} + \delta Q_{GL} + \sum_{k=1}^{N} h_{Lin_k} dm_{Lin_k} - h_L \sum_{k=1}^{N} dm_{Lout_k} + h_G'' dm_{ev} = dH_L - V_L dp \tag{5.8}$$

Here, δQ_{SL} is the heat exchanged between the compressor walls and the liquid phase. The conservation of the ammonia concentration in the liquid phase can be described with the following formula:

$$d\left(m_L X_L\right) = \sum_{k=1}^{N} X_{Lin_k} dm_{L\,in_k} - X_L \sum_{k=1}^{N} dm_{L\,out_k} - dm_{ev_{NH_3}} \tag{5.9}$$

By rearranging the conservation equations (Eq. (5.4), Eq. (5.5), Eq. (5.8), Eq. (5.9), Eq. (5.10), and Eq. (5.10)) the governing equations for the model can be obtained, which describe the change in pressure, temperature, concentration and volume in relation to the male rotor angle. The differential equation for the pressure is the following:

$$\frac{dp}{d\phi} = \frac{1}{\left(\frac{\partial v_G}{\partial p}\right)_{T,X}} \left[\frac{v_G}{m_G} \left(\sum_{k=1}^{N} \left(\frac{dm_{G\,out}}{d\phi} \right)_k - \left(\sum_{k=1}^{N} \left(\frac{dm_{G\,in}}{d\phi} \right)_k - \left(\frac{dm_{ev}}{d\phi} \right) \right) + \frac{1}{m_G} \frac{dV_G}{d\phi} - \left(\frac{\partial v_G}{\partial X_G} \right)_{p,T} \frac{dX_G}{d\phi} \right] \tag{5.10}$$

The derivative of the gas temperature by the male rotor angle is obtained from the gas energy conservation equation (Eq. (5.5)) and it is the following:

$$\begin{aligned} \frac{dT_G}{d\phi} = & \frac{\frac{\delta Q_{SG}}{d\phi} - \frac{\delta Q_{GL}}{d\phi} + \sum_{k=1}^{N} \left(h_{Gin_k} - h_G\right) \left(\frac{dm_{G\,in}}{d\phi} \right)_k - \left(h_G - h_G''\right) \left(\frac{dm_{ev}}{d\phi} \right) - m_G \left(\frac{\partial h_G}{\partial X_G} \right)_{p,T} \frac{dX_G}{d\phi}}{m_G \left(\frac{\partial h_G}{\partial T_G} \right)_{p,X} + \frac{m_G T_G}{\left(\frac{\partial v_G}{\partial p} \right)_{T,X}} \left(\frac{\partial v_G}{\partial T_G} \right)_{p,X}^2} + \\ & + \frac{T_G \left(\frac{\partial v_G}{\partial T_G} \right)_{p,X}}{\left(\frac{\partial v_G}{\partial p} \right)_{T,X}} \frac{v_G \left[\sum_{k=1}^{N} \left(\frac{dm_{G\,out}}{d\phi} \right)_k - \sum_{k=1}^{N} \left(\frac{dm_{G\,in}}{d\phi} \right)_k - \frac{dm_{ev}}{d\phi} \right] + \frac{dV_G}{d\phi} - m_G \left(\frac{\partial v_G}{\partial X_G} \right)_{p,T} \frac{dX_G}{d\phi}}{m_G \left(\frac{\partial h_G}{\partial T_G} \right)_{p,X} + \frac{m_G T_G}{\left(\frac{\partial v_G}{\partial p} \right)_{T,X}} \left(\frac{\partial v_G}{\partial T_G} \right)_{p,X}^2} \end{aligned} \tag{5.11}$$

The mass of evaporated ammonia in Eq.(5.6) and Eq.(5.7) can be expressed in the following way:

$$dm_{ev_{NH_3}} = x_{ev} dm_{ev} \tag{5.12}$$

Here, x_{ev} is the equilibrium concentration of the saturated gas at liquid temperature. Introducing this

expression in the gas concentration equation, the relation between the derivative of the gas concentration and the male rotor angle is obtained:

$$\frac{dX_G}{d\phi} = \frac{\sum_{k=1}^{N} \left(X_{Gin_k} - X_G\right) \left(\frac{dm_{G_{in}}}{d\phi}\right)_k + \left(X_{ev} - X_G\right) \frac{dm_{ev}}{d\phi}}{m_G} \tag{5.13}$$

In order to find the pressure and gas temperature, the derivative of the gas volume is needed. The vapor volume is a function of the geometry of the compressor and of the liquid volume.

$$\frac{dV_G}{d\phi} = \frac{dV}{d\phi} - \frac{dV_L}{d\phi} \tag{5.14}$$

The derivative of the liquid can be developed in the following way:

$$\frac{dV_L}{d\phi} = v_L \frac{dm_L}{d\phi} + m_L \frac{dv_L}{d\phi} \tag{5.15}$$

In this formula, the specific volume of the liquid is only a function of the liquid temperature and concentration; it does not depend on pressure.

$$\frac{dV_L}{d\phi} = v_L \left[\sum_{k=1}^{N} \left(\frac{dm_{L_{in}}}{d\phi}\right)_k - \sum_{k=1}^{N} \left(\frac{dm_{L_{out}}}{d\phi}\right)_k - \frac{dm_{ev}}{d\phi} \right] + m_L \left[\left(\frac{\partial v_L}{\partial T_L}\right)_X \frac{dT_L}{d\phi} + \left(\frac{\partial v_L}{\partial X_L}\right)_T \frac{dX_L}{d\phi} \right] \tag{5.16}$$

From the differentiation of the energy conservation equation for the liquid, the derivative of the liquid temperature is obtained:

$$\begin{aligned} \frac{dT_L}{d\phi} = & \frac{\frac{\delta Q_{SL}}{d\phi} + \frac{\delta Q_{GL}}{d\phi} + \sum_{k=1}^{N} \left(h_{Lin_k} - h_L\right) \left(\frac{dm_{L_{in}}}{d\phi}\right)_k - \left(h_G'' - h_L\right) \frac{dm_{ev}}{d\phi}}{m_L \left(\frac{\partial h_L}{\partial T_L}\right)_{p,X}} + \\ & + \frac{T_L \left(\frac{\partial v_L}{\partial T_L}\right)_{p,X} \frac{dp}{d\phi} - \left(\frac{\partial h_L}{\partial X_L}\right)_{p,T} \frac{dX_L}{d\phi}}{\left(\frac{\partial h_L}{\partial T_L}\right)_{p,X}} \end{aligned} \tag{5.17}$$

Introducing Eq. (5.12) in the liquid concentration equation, the derivative of the liquid concentration can be written as:

$$\frac{dX_L}{d\phi} = \frac{\sum_{k=1}^{N} \left(X_{Lin_k} - X_L\right) \left(\frac{dm_{L_{in}}}{d\phi}\right)_k + \left(X_{ev} - X_L\right) \frac{dm_{ev}}{d\phi}}{m_L} \tag{5.18}$$

The five-point stencil algorithm was used to estimate the partial derivatives needed in the governing equations. This numerical technique is employed within finite volume and finite difference methods to approximate derivatives or address partial differential equations on a discrete grid. The first derivative of a function f with respect to a real variable at a specific point x, using h as spacing between points in the grid, can be approximated using the five-point stencil as:

$$f'(x) \approx \frac{-f\left(x+2h\right) + 8f\left(x+h\right) - 8f\left(x-h\right) + f\left(x-2h\right)}{12h} \tag{5.19}$$

Finally, the governing equations of the heterogeneous model are Eq. (5.18), (5.17), (5.16), (5.14), (5.13), (5.11) and (5.10).

5.3. Structure of the compressor model

The *compressor model* is structured into three main sections:

1. Computation of the geometrical curves of the compressor and leakage paths.
2. Computation of the physical properties assuming no leakages occur.
3. Computation of the physical properties accounting for leakages and heat transfer.

In the first block, the geometrical curves of the compressor are obtained and have been discussed in detail in section 5.1. In the second block, the first computation is performed excluding leakages and heat transfer. This is necessary for obtaining the values of pressure in the neighbouring cavities in order to account for leakages. In the third block the final computation is performed, accounting for leakages and heat transfer. This block computes the final outlet properties and the performance indices. In Figure 5.10, the structure for the compressor model is shown.

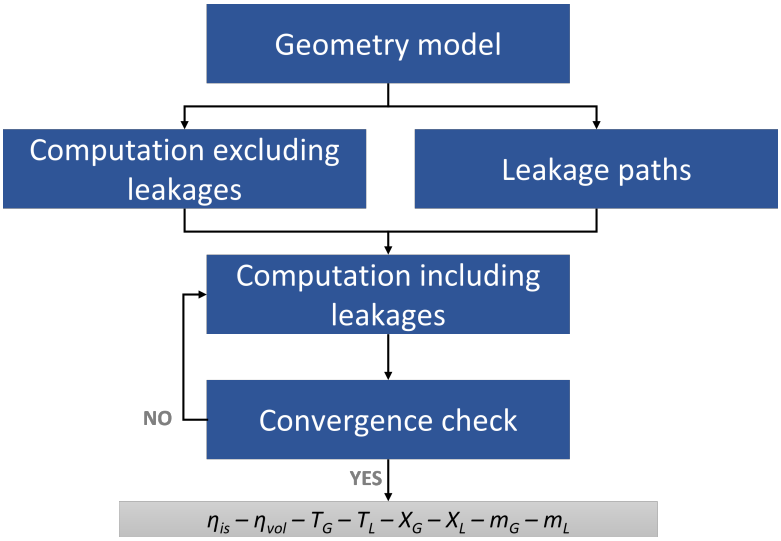

Figure 5.10: Structure for the compressor model.

5.3.1. Computation without leakages

Once all the geometrical features are calculated, the first computation is run. In this section, heat transfer and leakages are neglected. The purpose of this computation is to obtain the base values of the physical properties from which it is possible to build on the real physical properties vectors. This is necessary because, in order to calculate the leakages, the pressure in the neighbouring cavities must be known. In this section, the suction and discharge phase are assumed to be constant, while during compression the properties change. As a consequence, an initial mass in the compressor cavity can be estimated [Chamoun et al. (2013)].

$$m = \frac{V_{max}}{v_{suc}} \tag{5.20}$$

With the maximum total mass, it is possible to calculate the mass of the vapor and the mass of the liquid, when accounting for the vapor quality. These values are used in the computation of the pressure, specific volumes, temperatures and concentrations when using the equations described in section 5.2. The first section of the compressor model is not subjected to convergence.

5.3.2. Computation with leakages

The output properties from the first computation are used for initializing the properties in the second computation. In this case, the inlet mass in the compressor is computed with 5.20, using the suction cavity volume. During the compressor's operations several flows enter or leave the cavity volume.

These are the suction and discharge flows and the internal leakages. The masses in each control volume are evaluated using the continuity equation:

$$\frac{dm}{d\phi} = \frac{\zeta A w}{\omega v} \tag{5.21}$$

Here ζ is an experimental flow coefficient, which differs for suction, discharge and leakage path, and A is the total minimal area normal to the flow velocity. Following a heterogeneous assumption, the liquid and the vapor flow velocity will be different, impacting the distribution of the two phases. This effect is accounted for using the void fraction, where S represents the slip ratio between the vapor and the liquid flow velocities.

$$\epsilon = \frac{1}{1 + \frac{1-Q}{Q}\left(\frac{\rho_G}{\rho_L}\right)S} \tag{5.22}$$

The void fraction is multiplied by the total area in Eq. (5.21) when computing the vapor mass, while its complement to unity is used when the liquid mass is computed. For the computation of the velocity the isentropic converging nozzle flow model is used. This model assumes that the flow is isentropic.

$$w = \sqrt{2\int_{p_{down}}^{p_{up}} v\, dp} \tag{5.23}$$

The flow velocity from the model is integrated between the upstream and downstream pressure; v is the specific volume of the considered phase. The velocity is set to be positive if the flow is flowing into the control volume, otherwise it is set to be negative. The maximum flow velocity that can be obtained in the converging nozzle is the local speed of sound:

$$w_{max} = v\sqrt{-\left(\frac{\partial p}{\partial v}\right)} \tag{5.24}$$

Therefore, if the velocity computed with Eq. (5.23) exceeds the local sound velocity of the flow computed with Eq. (5.24), the velocity is set to its maximum number. The velocity is computed both for liquid and vapor flow at the suction, at the discharge and in the leakage paths and used in Eq. (5.21) for the evaluation of the respective mass flow rates. The driving force for the leakage flows is the pressure difference between grooves adjacent to the working chamber. The inlet mass of the leakages is computed using Eq. (5.25), while the outlet mass is calculated using Eq.(5.26).

$$\frac{dm}{d\phi}_{in} = \frac{\zeta A\sqrt{2v_{\phi+\frac{2\pi}{z_1}}\left(p_{\phi+\frac{2\pi}{z_1}} - p_\phi\right)}}{\omega v_\phi} \tag{5.25}$$

$$\frac{dm}{d\phi}_{out} = \frac{\zeta A\sqrt{2v_\phi\left(p_\phi - p_{\phi-\frac{2\pi}{z_1}}\right)}}{\omega v_{\phi-\frac{2\pi}{z_1}}} \tag{5.26}$$

However, since this mass is computed under isentropic assumption, a modification coefficient (ζ) is used to account for non-isentropic effects. As previously mentioned, this coefficient differs for suction, discharge and leakage paths and it is usually derived from experimental data.

Once all the masses have been calculated, the heat transfer computation begins. Due to centrifugal forces, the liquid is pushed against the housing of the compressor, creating a net separation between the liquid and the vapor phase. Because of the high temperature difference, heat is transferred from the vapor to the liquid phase. This energy heats the liquid, potentially causing evaporation.

Due to the complex geometry of the twin-screw compressor, estimating the heat transfer area between the liquid and the vapor phase poses a challenge. Because of centrifugal forces, the liquid comes

in contact with the compressor housing, creating a film of thickness δ and width equal to the distance between the tips of two lobes of the rotor (see Figure 5.11). For each control volume, the thickness of the liquid film is calculated as a simple ratio between the liquid volume and the area occupied by the liquid. Below the liquid film, the vapor occupies the remaining volume of the cavity. The cross-sectional area of the cavity corresponding to the maximum volume can be imagined as a triangular shape of base d and side h. Based on this, the characteristic length for the liquid is the film thickness δ, while the characteristic length for the vapor is the hydraulic diameter, with area and perimeter equal to the cross-sectional area of the cavity and the perimeter of the cavity, respectively.

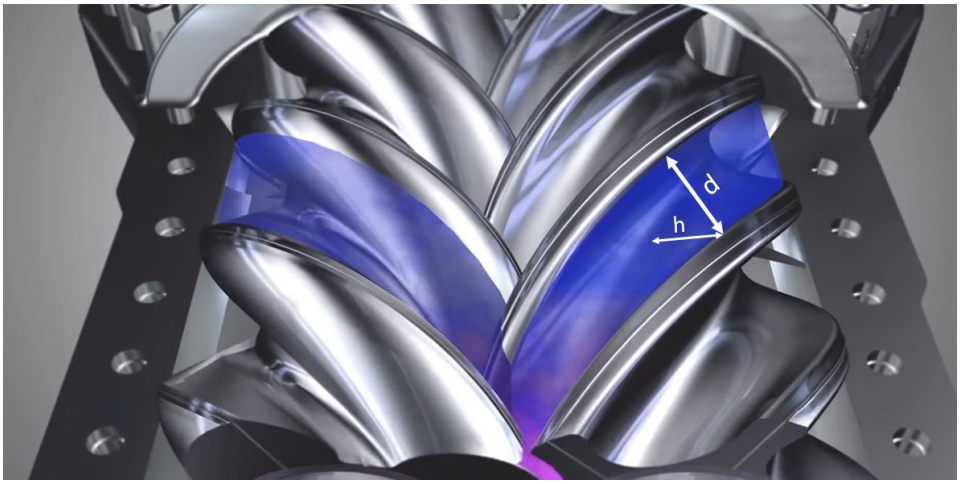

Figure 5.11: Area of heat transfer in a twin-screw compressor.

Depending on the state of the liquid, either sensible or latent heat transfer takes place. The temperature of the liquid is continuously compared to the saturation temperature of the liquid corresponding to that concentration and pressure. Since the pressure in the cavity rapidly increases, the liquid might reach a subcooled state. In this case, only sensible heat transfer occurs between the vapor and the liquid film, raising the temperature of the liquid until it returns to its saturation state. The overall heat transfer coefficient for sensible heat transfer considers both liquid and vapor heat transfer coefficients, which are computed based on the Reynolds number for both the vapor and the liquid flow. When the liquid reaches its saturation state, in addition to sensible heat transfer, also latent heat transfer occurs. In this case, a certain fraction of liquid evaporates, increasing the vapor content. This phenomenon decreases the concentration of ammonia in the liquid flow. The Kattan-Thome-Favrat correlation for multi-component zeotropic mixtures is used for the computation of the heat transfer coefficient [Thome (2004)]. The total heat transfer from the vapor to the liquid is computed using the following formula:

$$Q_{GL} = UA\Delta T_{ml} \tag{5.27}$$

Here, ΔT_{ml} is the logarithmic mean temperature difference. This formula is both used in the computation of the fluid properties in the equations explained in section 5.2 and for the computation of the evaporated mass flow rates, obtained using the following energy balance:

$$\dot{m}_{Lin}h_{Lin} + Q_{GL} = \dot{m}_{Lout}h_{Lout} + \Delta h_{vap}\dot{m}_{ev} \tag{5.28}$$

The evaporated mass is subtracted from the liquid mass and added to the vapor mass if positive, while a negative value indicates condensation and therefore it is added to the liquid mass and subtracted from the vapor mass. Equations in section 5.2 are implemented in order to obtain the inlet properties in the next control volume. The process is repeated for all the control volumes until convergence is achieved. Convergence is determined based on the difference in pressure between two consecutive simulations at a specific point, which is chosen before the discharge port opens.

When convergence is achieved, the compressor performance is analyzed. First the mass flow rate is calculated using the following formula:

$$\dot{m} = z_1 \frac{n}{60} \int \frac{\partial m}{\partial \phi} d\phi \tag{5.29}$$

The total mass flow rate is used in the computation of the isentropic compression power using the following equation:

$$\dot{W}_{is} = \dot{m}\,(h_{is} - h_{suc}) \tag{5.30}$$

Here, h_{is} is the discharge enthalpy under isentropic compression, which is determined as a function of the pressure, the mixture concentration at the discharge and the specific entropy at the suction. The indicated power is the compression power input excluding mechanical and motor losses and it is computed using the following formula:

$$\dot{W}_{ind} = z_1 \frac{n}{60} \int p dV \tag{5.31}$$

The isentropic efficiency is the ratio between the isentropic and compression power, including losses.

$$\eta_{is} = \frac{\dot{W}_{is}}{\dot{W}_{comp}} \tag{5.32}$$

The motor efficiency is a fixed factor, set at 93%. The mechanical efficiency is computed for each set of experimental data and given as input to the model. The volumetric efficiency is expressed as ratio between the real and theoretical volumetric displacement.

$$\eta_{vol} = \frac{v_{suc} \int \frac{\partial m}{\partial \phi} d\phi}{V_{max}} \tag{5.33}$$

5.4. Overall model structure

In order to find the most realistic model, the *compressor model* is integrated with three other models. The first model, hereafter referred to as the "*input data model*", is explained in section 7.3 and provides the right input parameters for the *compressor model*. The second model, hereafter referred to as the "*discharge pipe data model*", is described in section 5.5 and recreates the compressed flow once it exits the compressor and is mixed in the pipe. The third model, hereafter referred to as the "*cycle model*", is discussed in section 5.6. The *input data model* recreates the inlet conditions at the suction side of the compressor. Here, there is an additional mass flow rate coming from the gap seal which modifies the suction properties of the flow at the inlet of the compressor. The different input parameters for the *input data model* are:

- The pressure and the temperature of the mixture at the inlet of the compressor measured with the sensors.
- The discharge pressure and the discharge temperature of the mixture measured with the sensors.
- The flow rates at the inlet of the compressor measured with the sensors and adjusted to account for the flashing of the liquid.
- The motor power.

The *input data model* returns as output the inlet temperature, the vapor quality at the suction and the mass flow rate coming from the gap seal.

The input for the *discharge pipe data model* are obtained through the *compressor model* and are:

- The discharge temperature of the liquid and of the vapor.
- The discharge pressure.
- The mass flow rates of the liquid and of the vapor.
- The discharge specific enthalpy of the liquid and of the vapor.

The *discharge pipe data model* investigates the mixing and the heat transfer between the liquid and the vapor phase in the pipe at the outlet of the compressor. In Figure 5.12, a flow chart for the overall model structure is shown.

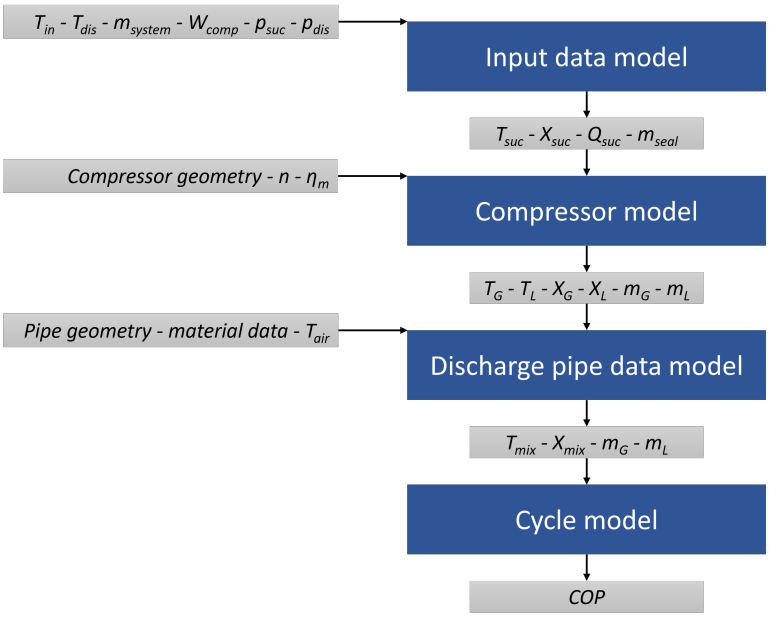

Figure 5.12: Overall model structure.

5.5. Discharge pipe data model

At the end of the compression process, the liquid and the vapor phase might not be in equilibrium yet. The vapor might be superheated, exhibiting higher temperatures than the liquid and creating a temperature distribution across the flow. Most probably, heat transfer between the vapor and the liquid phase still occurs until the mixture reaches equilibrium conditions again. In order to evaluate the properties of the compressed mixture, the model of the pipe is developed. In this model, the heat transfer between the vapor and liquid is computed. First, the flow regime is checked in order to calculate the characteristic length scale of the liquid flow and the interfacial area between vapor and liquid. Secondly, the saturation state of the liquid is checked. If the liquid is subcooled, then only sensible heat transfer occurs. Once the liquid reaches its saturation temperature, latent heat transfer occurs between the vapor and the liquid. Heat losses to the environment and pressure drop in the pipe are taken into account.

This model is also necessary for the validation of the model with experimental data. The temperature sensor at the discharge side is placed approximately 1.3 m after the compressor. According to Kothari (2020), following the heterogeneous assumption, the sensor measures only the temperature of the liquid. Another possibility involves that the liquid and the vapor flow reach equilibrium conditions. This state is reached through heat transfer, causing a reduction in the temperature of the superheated vapor. The *discharge pipe data model* is supplied with output values obtained from the *compressor model*. The input properties are the temperatures of the vapor and of the liquid, the discharge pressure, the mass flow rates and the ammonia concentration in both phases. These are given considering that the mass flow from the gap seal is removed from the total flow. This model is based on the following assumptions:

- The mixture is heterogeneous at the inlet of the pipe.
- The pipe is considered as entirely horizontal.
- Instability in the pipe bends is neglected.

The model employs a finite control volume approach: the length of the pipe is discretized in 10000 control volumes of infinitesimal length dx. Forward differentiation is used; the outlet properties of one control volume are assigned as input properties for the next control volume. The pressure drop in the pipe is the sum of three contributions: the static pressure drop, the momentum pressure drop and the frictional pressure drop. In this case, the static pressure drop is neglected as it is caused by a change

in static head. For simplification, the entire tube is assumed to be horizontal, despite the deviation from the real case. The momentum pressure drop is caused by the change in kinetic energy of the flow:

$$\Delta p_{mom} = \dot{m}^2 \left\{ \left[\frac{(1-Q)^2}{\rho_L (1-\epsilon)} + \frac{Q^2}{\rho_G \epsilon} \right]_{out} - \left[\frac{(1-Q)^2}{\rho_L (1-\epsilon)} + \frac{Q^2}{\rho_G \epsilon} \right]_{in} \right\} \tag{5.34}$$

For the frictional pressure drop, the correlation method proposed by Friedel (1979) is implemented. The heat transfer coefficient for double phase flow is based on the correlation proposed by Zhang et al. (2019) for flow boiling of zeotropic mixtures in horizontal plain tubes. If the liquid is at saturation conditions, the heat transfer between the liquid and vapor causes evaporation of the liquid. Therefore, at each control volume, the evaporated mass flow rate is computed through an energy balance on the vapor or on the liquid phase. Figure 5.13 displays the heat transfer rates which occur in a control volume.

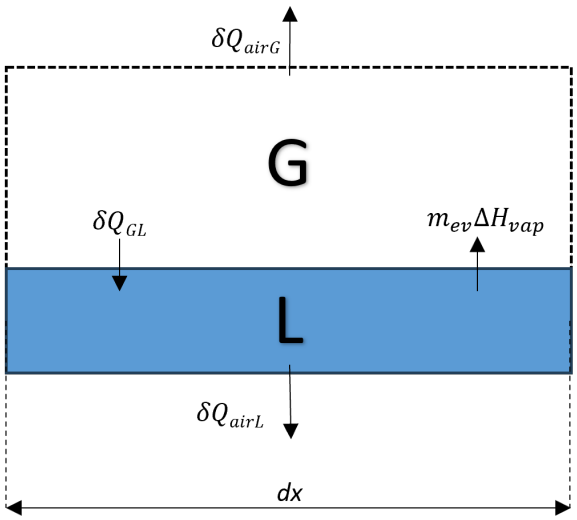

Figure 5.13: Heat transfer rates in a control volume.

The heat transfer between the vapor flow, the liquid flow and the air differs due to variations in heat transfer areas and the temperatures of the two phases. Unless equilibrium conditions are reached, the vapor still has a higher temperature than the liquid phase. Generally, working with a vapor quality larger than 50%, the area occupied by the vapor is larger than the area occupied by the liquid. The cross-sectional area occupied by the liquid phase is computed using the void fraction:

$$A_L = A\,(1-\epsilon) \tag{5.35}$$

Here, A is the total cross-sectional area of the pipe. If the flow is fully stratified then the angle θ_1 is given from Thome (2004):

$$A_L = 0.5 r_i{}^2\,[(2\pi - \theta_1) - sin\,(2\pi - \theta_1)] \tag{5.36}$$

From θ_1 the side wet and dry areas are obtained. These values are used for estimating the heat losses to the environment. Specifically, the heat transfer modes considered here are convection and conduction, while radiation is neglected. In addition, the wet diameter at the interface between vapor and liquid is computed to obtain the heat transfer area at the interface. Through simple mass, concentration and energy balances the properties for the next control volume are updated.

5.6. Cycle model

The *cycle model* is used to compute the COP for the heat pump. The model is based on the following assumptions:

- The heat pump runs in steady state.

- The pressure drop in the heat exchangers is neglected.
- The flow at the exit of the absorber is saturated liquid.
- The expansion process is assumed to be isenthalpic.

The output data of the *discharge pipe data model* are fed to the *cycle model* (discharge temperature, specific enthalpy, ammonia concentration and mass flow rates). For clarity, the thermodynamic states in the heat pump cycle are defined in the following way:

- *State 1*: the working fluid exits the desorber and enters in the compressor.
- *State 2*: the working fluid is discharged from the compressor and enters in the absorber.
- *State 3*: the working fluid exits from the absorber and enters in the expansions valve.
- *State 4*: the working fluid is expanded and enters in the desorber.

As mentioned in the assumptions, the flow at the outlet of the absorber is saturated liquid, therefore the enthalpy can be determined as a function of the system high pressure (p_2) and of the vapor quality (Q) at a specific ammonia concentration (X_{cycle}):

$$h_3 = f(p_2, Q = 0, X_{cycle}) \tag{5.37}$$

The heat transfer through the absorber is computed with the following relation:

$$\dot{Q}_{abs} = \dot{m}_{cycle}(h_2 - h_3) \tag{5.38}$$

The compressor power is provided by the *compressor model*, hence the COP is computed with Eq. (2.2). The process through the expansion valve is assumed to be isenthalpic. This means that the enthalpy in state 4 has the same value of the specific enthalpy in state 3. From Eq. (2.1), the heat transfer in the desorber is obtained. The specific enthalpy in state 1 is computed with the following relation:

$$h_1 = h_4 + \frac{\dot{Q}_{des}}{\dot{m}_{cycle}} \tag{5.39}$$

From the specific enthalpy at state 1, the temperature at the inlet of the compressor, before the system flow is mixed with the flow coming from the gap seal, can be computed with the following relation:

$$T_1 = f(p_1, h_1, X_{cycle}) \tag{5.40}$$

6

Model validation

The model is validated with the experimental data obtained in 2020 by Kothari (2020). However, some of these data sets are regenerated considering an additional flow at the inlet of the compressor. Several input parameters, such as rotational speed, vapor quality, suction pressure and pressure ratio, are varied in order to analyze their impact on the compressor's performance.

6.1. Preparation of experimental data

The raw experimental data were provided to a MATLAB model (formulated to process the experimental data) based on mass, energy and species balances to compute all the missing properties and performance indices. The computation developed by Kothari (2020) was adapted here. It is necessary to account for the change in the composition of the mixture when the liquid undergoes flash vaporization while passing through the expansion valve. This process likely generates a fraction of vapor, which adds to the vapor flow, thus changing the vapor quality at the inlet of the compressor. The inlet conditions at the compressor are further impacted by the flow coming from the gap seal. These flows were neglected in the work of Kothari (2020). Nevertheless, they do impact the performance of the cycle. The MATLAB model for processing the experimental data follows the explained procedure. Refer to Figure 6.1 for the nomenclature of the measurement sensors. The liquid and the vapor concentration after the separator are computed, assuming that they are in equilibrium within the separator:

$$X_{Gsep} = f(T_{405}, p_{404}, Q = 1) \tag{6.1}$$

$$X_{Lsep} = f(T_{405}, p_{404}, Q = 0) \tag{6.2}$$

The vapor and liquid specific enthalpies after the separator are computed using the following equations:

$$h_G = f(T_{802}, p_{402}, X_{Gsep}) \tag{6.3}$$

$$h_L = f(T_{801}, p_{401}, X_{Lsep}) \tag{6.4}$$

Before going through the expansion valve, the liquid flow rate is measured by a flow meter (FT-401). This flow meter requires the liquid temperature to be within a certain range. Therefore, the liquid is cooled down in a subcooler before reaching FT-401. The inlet liquid specific enthalpy at the subcooler is computed using the following relation:

$$h_{sub_{in}} = f(T_{405}, p_{404}, X_{Lsep}) \tag{6.5}$$

The heat transfer in the subcooler is quantified with the following formula:

$$\dot{Q}_{sub} = \dot{m}_{cw} cp_{cw} (T_{721} - T_{720}) \tag{6.6}$$

The outlet specific enthalpy of the liquid flow is computed through the energy balance on the subcooler:

$$h_{sub_{out}} = h_{sub_{in}} - \frac{\dot{Q}_{sub}}{\dot{m}_L} \tag{6.7}$$

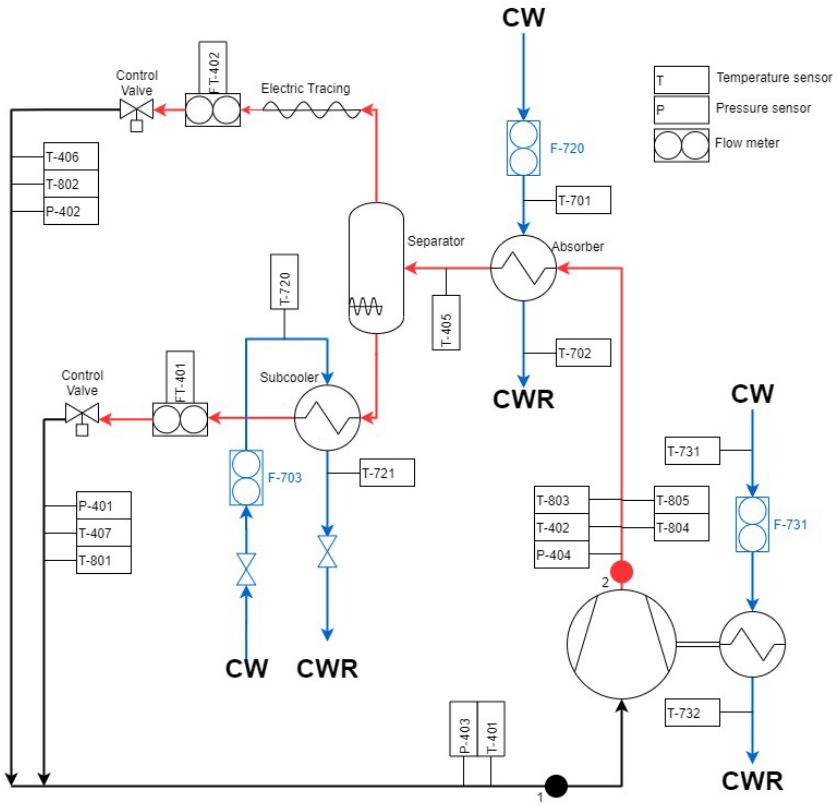

Figure 6.1: Schematic representation of the experimental setup and sensor nomenclature. Figure from Kothari (2020).

After the subcooler, the liquid is expanded to suction pressure. The process is isenthalpic, and as such the specific enthalpy at the outlet of the expansion valve has the same value as the one measured after the subcooler. In this case, the experimental values measured by the sensors (T_{407} and T_{801}) after the expansion valve are not taken into account. At this position, the temperature is strongly affected by the tube temperature due to the low liquid flow rate and the low velocity. Therefore, the temperature of the liquid after expansion is computed with the following formula:

$$T_{L_{after,flash}} = f(p_{401}, h_{sub_{out}}, X_{Lsep}) \tag{6.8}$$

In this way, it is possible to calculate the amount of vapor produced during flashing:

$$h_{Gsat} = f(T_{L_{after,flash}}, p_{401}, Q = 1) \tag{6.9}$$

$$h_{Lsat} = f(T_{L_{after,flash}}, p_{401}, Q = 0) \tag{6.10}$$

$$Q_{flash} = \frac{h_{subout} - h_{Lsat}}{h_{Gsat} - h_{Lsat}} \tag{6.11}$$

Hence, the new mass flow rates approaching the inlet of the compressor can be computed as such:

$$\dot{m}_L = (1 - Q_{flash})\dot{m}_L \tag{6.12}$$

$$\dot{m}_G = \dot{m}_G + Q_{flash}\dot{m}_L \tag{6.13}$$

The new concentration of the liquid is obtained and with it the inlet specific enthalpy and density:

$$X_{L_{in}} = f(T_{L_{after,flash}}, p_{403}, Q = 0) \tag{6.14}$$

$$h_{L_{in}} = f(T_{L_{after,flash}}, p_{403}, X_{L_{in}}) \tag{6.15}$$

$$\rho_{L_{in}} = f(T_{L_{after,flash}}, p_{403}, X_{L_{in}}) \tag{6.16}$$

In the same way, it is possible to obtain the concentration, the specific enthalpy and the density of the vapor flow.

6.1.1. Input data model

As previously mentioned, there is another flow at the inlet of the compressor, which comes from the gap seal at the high pressure side. This mass flow rate was not measured in the previous experiments and therefore it was estimated. This flow is predominantly vapor and shares the same concentration as the discharge vapor flow. When it mixes with the suction flow, it increases the composition, vapor quality, and temperature at the compressor's inlet. Therefore, all the experimental input values recorded in the work of Kothari (2020) were adjusted to account for the influence of the flow from the seal on the input conditions. The mass flow rate from the seal is estimated by using of the nozzle flow equation:

$$\dot{m}_{seal} = C_{seal}\sqrt{2\rho_{seal}(p_{dis} - p_{suc})} \tag{6.17}$$

Here, C_{seal} is an experimental flow coefficient, which was estimated by Ferreira (2023). In Figure 6.2, a graphical representation of the models and the mass coming from the gap seal can be visualized.

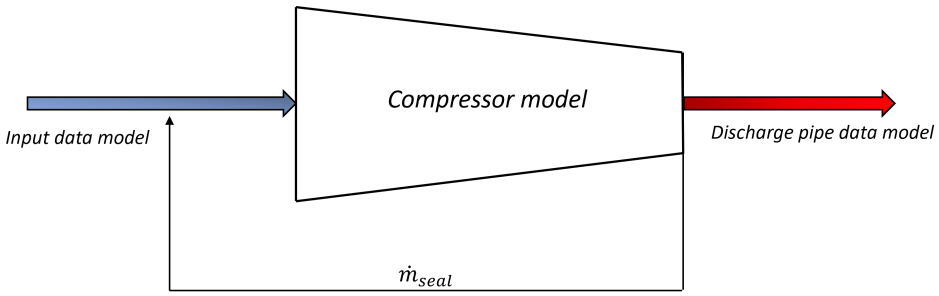

Figure 6.2: Graphical representation of the mass coming from the gap seal. Inspired by Ferreira (2023).

In order to compute the mass flow rate from the gap seal, it is necessary to compute the density of this flow. Some assumptions are made in the following computation:

- The liquid and vapor flow are saturated at the suction.
- The liquid flow is saturated at the discharge.
- The vapor flow is superheated at the discharge.
- The ammonia concentration in the vapor flow is assumed to be unchanged in the first iteration.
- The liquid vaporizes increasing the vapor content.
- The flow from the seal is predominantly vapor and has the same concentration of the vapor flow at the compressor's discharge.

The mass flow rate of the liquid at the discharge can be obtained with a species balance for the liquid phase.

$$\dot{m}_{Lout} = \dot{m}_{Lin}\frac{X_{G\,out} - X_{Lin}}{X_{G\,out} - X_{L\,out}} \tag{6.18}$$

The vapor concentration at the discharge can be obtained from the species balance for the vapor phase.

$$X_{G\,out} = \frac{\dot{m}_{Gin}X_{G\,in} + \dot{m}_{Lin}X_{G\,out} - \dot{m}_{Lout}X_{G\,out}}{\dot{m}_{Gin} + \dot{m}_{Lin} - \dot{m}_{Lout}} \tag{6.19}$$

The procedure is iterated until convergence is achieved. The properties of the flow from the gap seal are computed considering the discharge properties of the vapor phase. The specific enthalpy of the vapor at the discharge can be obtained from the energy balance:

$$h_{G\,out} = \frac{\dot{m}_{Tin}h_{T\,in} + \dot{W}_{comp} - \dot{m}_{Lout}h_{L\,out}}{\dot{m}_{Gin} + \dot{m}_{seal} + \dot{m}_{Lin} - \dot{m}_{Lout}} \tag{6.20}$$

The total mass flow rates and the total specific enthalpy at the suction are computed with the following balances:

$$\dot{m}_{Tin} = \dot{m}_{Lin} + \dot{m}_{Gin} + \dot{m}_{seal} \tag{6.21}$$

$$h_{Tin} = \frac{\dot{m}_{Lin} h_{Lin} + \dot{m}_{Gin} h_{Gin} + \dot{m}_{seal} h_{seal}}{\dot{m}_{Tin}} \tag{6.22}$$

The vapor outlet temperature is computed using the vapor specific enthalpy obtained in Eq. (6.20).

$$T_{G_{out}} = f(p_{dis}, X_{G_{out}}, h_{G_{out}}) \tag{6.23}$$

This temperature is used to recalculate the density and the specific enthalpy of the seal, resulting in a more precise estimate of the mass flow rate from the gap seal. Once the value of the mass flow rate from the gap seal is determined, it is used to calculate the new ammonia concentration of the mixture at the inlet of the compressor, as well as the new inlet temperature. These values serve as input for the *compressor model*. Additionally, during this work, the experimental volumetric and isentropic efficiencies were recalculated taking into account this flow.

6.2. Comparison with experimental data

In order to validate the aforementioned models, several data sets obtained from the experimental work of Kothari (2020) were processed and compared with the results obtained with the numerical models. As previously mentioned, some of these data within these data sets were modified before being implemented in order to account for the flow from the gap seal. The rotational speed in the different data sets varies between 9030 rpm and 14205 rpm, while the pressure ratio between 1.9 and 3.3. The conditions closely resemble each other because the experimental temperature in the absorber was limited to approximately 100°C due to deposition of fouling on the water side of the absorber at higher temperatures.

For the validation of the model, the experimental values of isentropic and volumetric efficiency were compared with the values obtained from the *compressor model*. Because the model does not account for heat and friction losses, the isentropic efficiency is expected to be higher than the experimental values. Additionally, the pipe after the compressor was modelled to clarify to which fluid the measured temperature at the discharge side of the compressor corresponds. If the liquid and the vapor are in equilibrium at that point, the measured temperature is the temperature of the mixture. Otherwise, according to the hypothesis of Kothari (2020), the measured temperature might correspond to the temperature of the liquid phase.

The experimental and simulated isentropic efficiency are shown in Figure 6.3.

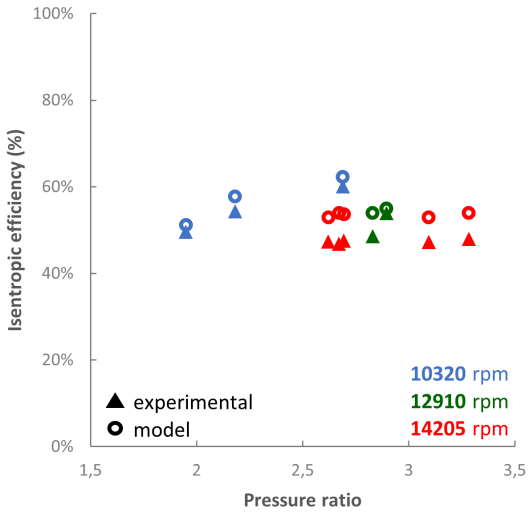

Figure 6.3: Experimental validation of the isentropic efficiency for different rotational speeds and pressure ratios.

It can be observed that for low rotational speed (10320 rpm) the accuracy of the model prediction is quite high, with a mean error of 4%. When increasing the rotational speed (12910 rpm) the inaccuracy of the simulated results increases, showing a mean error of 6.5%. The highest inaccuracy occurs at higher rotational speeds (14205 rpm), with a mean error of 10.5%. This behavior is not uncommon when validating compressor models and can originate from the following reasons:

- The compressor is assumed adiabatic. No heat losses occur with the environment. In reality, at higher rotational speed, these losses would likely increase.
- The experimental flow coefficient used in the computation of the mass flow rates are usually obtained experimentally by getting the best fit of the analytic results to the experimental data for a certain set of operating conditions. This means that if the flow coefficients used in this work are tested for rotational speed up to 10000 rpm, they may fail beyond this limit.
- The motor efficiency in this work is assumed constant due to lack of correlations specific to the motor. However, the motor efficiency decreases with increasing rotational speeds.
- The different clearances for the leakage paths have the same size. In reality, each leakage path might have a different size of clearance. Specifically, at higher rotational speeds some leakage paths might play a bigger role and would hence reduce the efficiency. This effect cannot be accounted for in the model due to missing geometrical data.

Finally, it is important to take measurements errors and simulation approximations into account.

The volumetric efficiency does not exhibit the same trend as the isentropic efficiency (Figure 6.4). At low rotational speeds (10320 rpm) the accuracy of the model prediction is the lowest, with a mean error of 4.3%. When increasing the rotational speed (12910 rpm) the accuracy of the simulated results increases, showing a mean error of 2.3%. At the highest rotational speed (14205 rpm) the mean error is 2.8%.

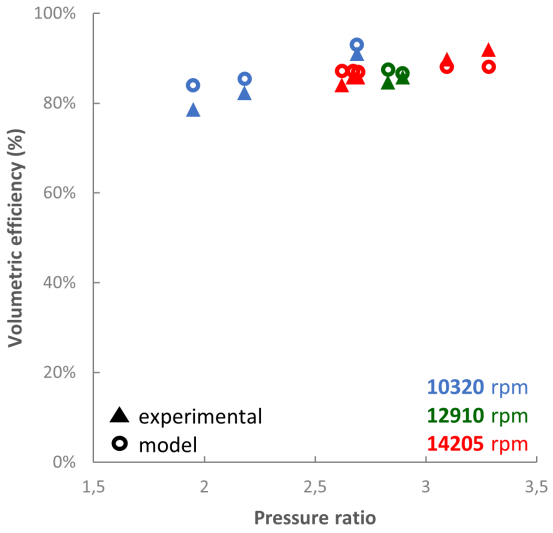

Figure 6.4: Experimental validation of the volumetric efficiency for different rotational speeds and pressure ratios.

The creation of the *discharge pipe data model* aimed to evaluate how the placement of the sensor within the setup affects the measured temperature. In each dataset, equilibrium between the vapor and liquid phases was not achieved at that specific point. A temperature difference persisted between the vapor and the liquid, and in the majority of cases, the temperature of the liquid at that location corresponded to the temperature measured by the sensor. In Figure 6.5, the measured temperatures and the simulated liquid temperatures are shown for the all data sets as a function of the pressure ratio.

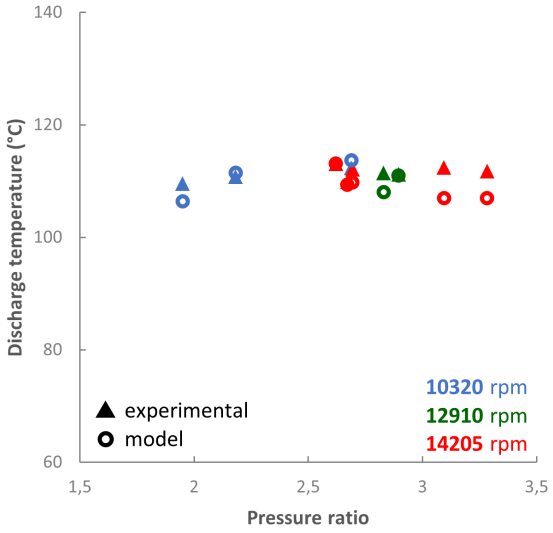

Figure 6.5: Experimental validation of the discharge temperature for different rotational speeds and pressure ratios.

6.2.1. Model discussion based on random data set

The results from data set 6 are discussed among others. In Figure 6.6, the evolution of the pressure for one cavity is shown as a function of the male rotor angle. From this picture, it is evident that over-compression occurs before the discharge phase begins. This happens because the compressor is not operating under ideal conditions. In addition, it is essential to keep in mind that the discharge conditions of the experimental compressor, e.g. opening/closing time and size of the port, are unknown, but the discharge conditions from the reference compressor are used. This means that some imperfections may occur during compression operations within the numerical model.

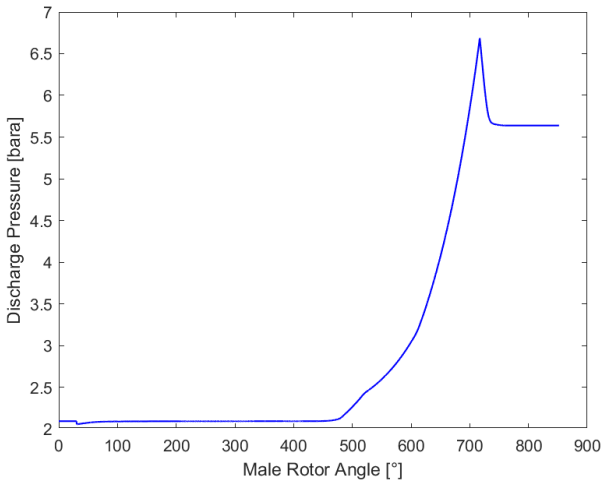

Figure 6.6: Evolution of the pressure as a function of male rotor angle for data set 6.

For data set 6, a 23.8 g/s mass flow rate from the gap seal is mixed with the working fluid at the input of the compressor, significantly impacting the temperature and the vapor quality at the suction. At the inlet of the compressor, both the liquid and the vapor are saturated and they continuously exchange heat, maintaining the same temperature during the entire suction phase. The temperature variation is primarily driven by the heat exchange since the variation in pressure is minimal during this phase.

As compression starts, the vapor becomes superheated since its temperature follows the trend of the pressure (Figure 6.6). The liquid is compressed and it becomes slightly subcooled. At this point, there is no latent heat transfer and the rate of heat transfer between the vapor and the liquid diminishes.

During the discharge phase, a large difference between the two temperatures is observed (Figure 6.7a). After the *compressor model*, the *discharge pipe data model* starts. The model takes as input data the output from the *compressor model* and calculates the pressure drop, the heat transfer between vapor and liquid, the heat loss between the vapor and the liquid with the external environment.

In Figure 6.7b, the vapor, liquid and mixture equilibrium temperatures are shown along the pipe length. The temperatures of the two phases approach each other as heat transfer occurs. The equilibrium temperature (in green) is closer to the temperature of vapor as the ammonia concentration in the mixture is higher than the water concentration.

At a distance of approximately 1.3 meters downstream from the compressor's discharge point, a temperature sensor is positioned. At this specific location, it is important to note that the liquid and vapor phases have not reached a state of equilibrium yet, as there is a temperature difference between the two phases. Here, the experimental discharge temperature exactly matches the temperature of the liquid, confirming the hypothesis that the measured temperature corresponds to the liquid temperature. This is observed for almost all data set, validating the *discharge pipe data model* as well.

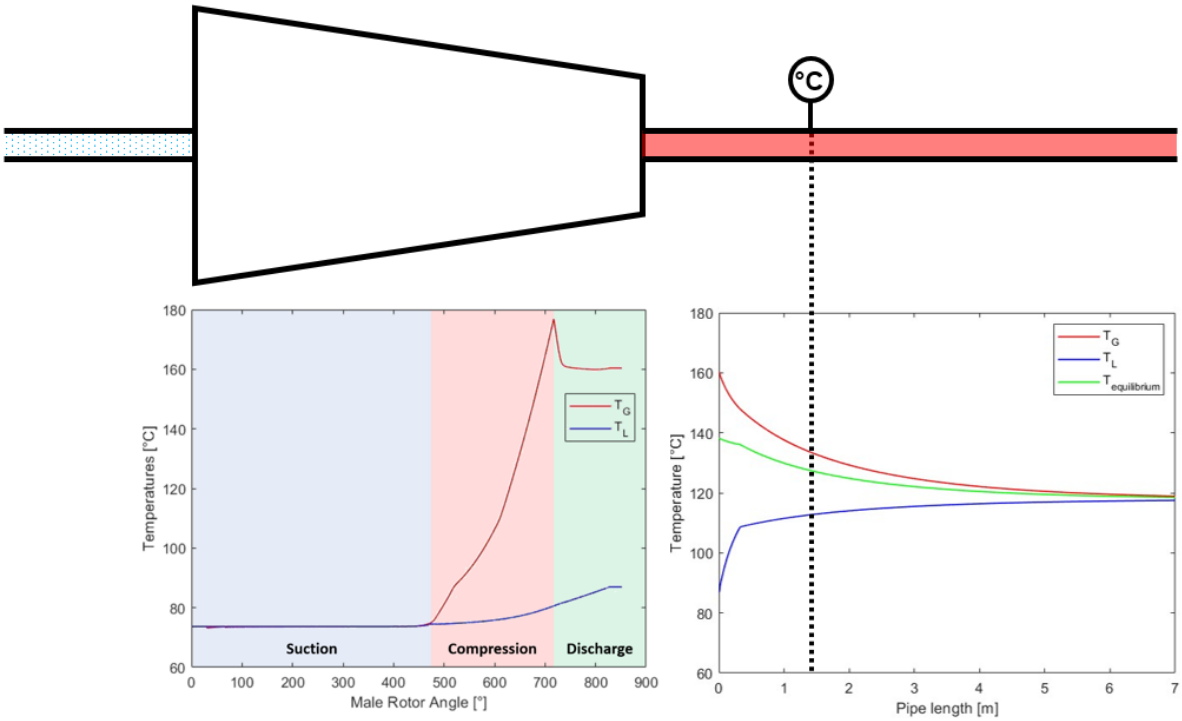

Figure 6.7: Evolution of the vapor and liquid phase temperature in the compressor (a) and in the discharge pipe (b) for data set 6.

In Table 6.1, the results from the model and the experimental data for data set 6 are compared.

Table 6.1: Comparison between experimental data and results from the model for data set 6.

	η_{is}	η_{vol}	T_{dis} [°C]
Experimental	0.6012	0.91	112.337
Model	0.6228	0.93	113.5
Difference	3.6 %	2%	1.1631 °C

7

Computational experimentation

Even though the experiments provided a comprehensive view of the compressor's performance under specific conditions, they did not offer further insights into which sink temperatures the CRHP could reach without compromising the system's efficiency. As previously mentioned, the operating conditions were set in order to limit the discharge temperature to approximately 100 °C, due to the fouling on the water side of the plate heat exchanger, which precluded its functioning. Here, a compressor model can assist in exploring several operating conditions which cannot be tested experimentally. The primary objective of this chapter is to investigate which operating conditions would maximize the compressor's efficiency within a specified range of conditions.

For each case, the discharge pressure and the rotational speed were fixed, while the suction temperature, pressure ratio and vapor quality were varied. When dealing with a pure fluid, only four parameters need to be fixed: the pressure ratio, the suction or discharge pressure, the rotational speed and the suction temperature. In this study, it is important to consider that when the compressor operates with a mixture there is one additional degree of freedom which has to be given as input, e.g. the inlet vapor quality or the ammonia concentration in the mixture. Therefore, in each simulation five parameters were fixed and one was varied.

The suction temperature and the vapor quality were given already taking into account that there is a flow from the gap seal which increases these two parameters. Since the input was given already considering the impact of this flow, the *inlet pipe model* was not adopted anymore, but the mass of the seal was computed at the end of the *compressor model*. The operating conditions at the inlet of the compressor (before the main flow from the desorber is mixed with the flow from the gap seal) are obtained through the *cycle model*. The effect of the flow from the gap seal on the COP of the heat pump was investigated and is discussed in this chapter. For all the investigated cases discussed in section 7.2 and 7.3, the compressor operated at 10320 rpm. This rotational speed was applied because the model validation with experimental data showed the highest accuracy at this speed.

7.1. Variation of the performance with pressure ratio

Before starting the investigation of the operating conditions, a broad range of pressure ratios was tested to identify the ideal pressure ratio at which the compressor should operate. The design pressure ratio of the experimental compressor should be approximately 3. However, since the geometry of the experimental compressor was slightly modified, the following investigation should give an indication at which pressure ratio the digital compressor should operate to maximize the performance. Here, the suction pressure, the suction temperature and the inlet vapor quality were fixed, while the rotational speed and the pressure ratio were varied. The suction pressure is set at 2 bara, since the limit for the gap seal of the compressor was set just above 1 bara.

In Figure 7.1, the isentropic efficiency is shown as a function of the pressure ratio at three different rotational speeds: 9030 rpm, 10320 rpm and 12910 rpm. The results of the model align with the overall trend of these parameters as the pressure ratio changes, reinforcing the model's validation. As expected, the isentropic efficiency follows a parabolic trend. The trend is similar for all three rotational

speeds. At pressure ratios lower than 2.5, the isentropic efficiency is quite low compared to the other values. It keeps increasing until a pressure ratio of 3.1 and then it slightly decreases. The optimal pressure ratio shifts to higher pressure ratios when higher rotational speeds are adopted, as confirmed by Yanagisawa et al. (1990). The data suggest that the isentropic efficiency assumes the highest value for a rotational speed equal to 10320 rpm.

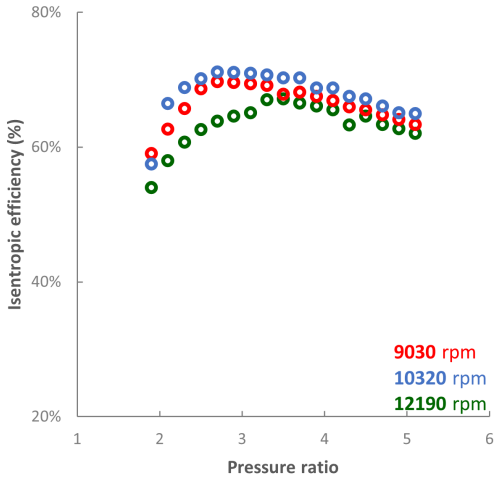

Figure 7.1: Isentropic efficiency as a function of pressure ratio and rotational speed.

Since the compressor's design is optimized for achieving the highest isentropic efficiency, from this investigation it can be deducted that the design pressure ratio of the digital compressor is to be found in a range between 2.9 and 3.2. Hence, the following investigation will be conducted at a pressure ratio equal to 3. As such, the best operating conditions can be analyzed if the compressor was to work at its design pressure ratio.

The volumetric efficiency is quite stable when varying the pressure ratio (Figure 7.2).

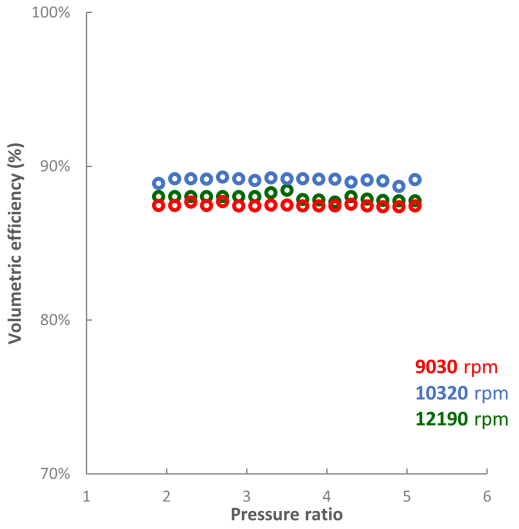

Figure 7.2: Volumetric efficiency as a function of pressure ratio and rotational speed.

The data suggest that the volumetric efficiency is relatively constant when the pressure ratio is varied. The volumetric efficiency is highest at a rotational speed of 10320 rpm and assumes the lowest value at the lowest rotational speed (9030 rpm). This well agrees with literature: the volumetric efficiency increases with the rotational speed, due to larger flow rate, until a maximum is reached.

7.2. Influence of the inlet vapor quality

The inlet vapor quality was varied between 80% and 98%. This parameter already accounts for the impact that the flow from the gap seal has on the inlet flow of the compressor. Hence, the inlet vapor quality of the flow coming from the rest of the system will be lower. High inlet vapor qualities were not only chosen to consider the effect of the seal, but also because Van De Bor et al. (2014) stated that, in the optimal case, the outlet vapor quality at the compressor's discharge should be 1, regardless of the ammonia concentration. However, setting values of inlet vapor qualities near unity increases the possibility that the vapor reaches high superheating, so it is important to mediate this parameter.

In Figure 7.3, the isentropic efficiency is plotted as a function of inlet vapor quality. The general trend suggests that the isentropic efficiency increases with rising the inlet vapor quality. Yet, an initial marginal decrease in isentropic efficiency is noted.

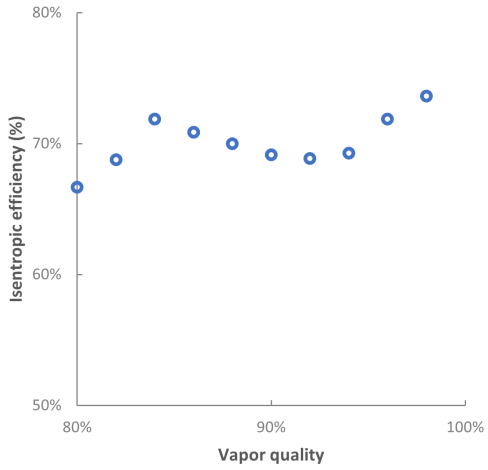

Figure 7.3: Isentropic efficiency as a function of the inlet vapor quality.

In order to explain the reasons behind this specific behavior of the isentropic efficiency, both the real and isentropic compressor power were analyzed. Figure 7.4a indicates a similarity between the trends of the isentropic power and isentropic efficiency, while the real compression power (Figure 7.4b) is less affected by the inlet vapor quality. When compared to the compression power, the isentropic power has the largest impact on the isentropic efficiency.

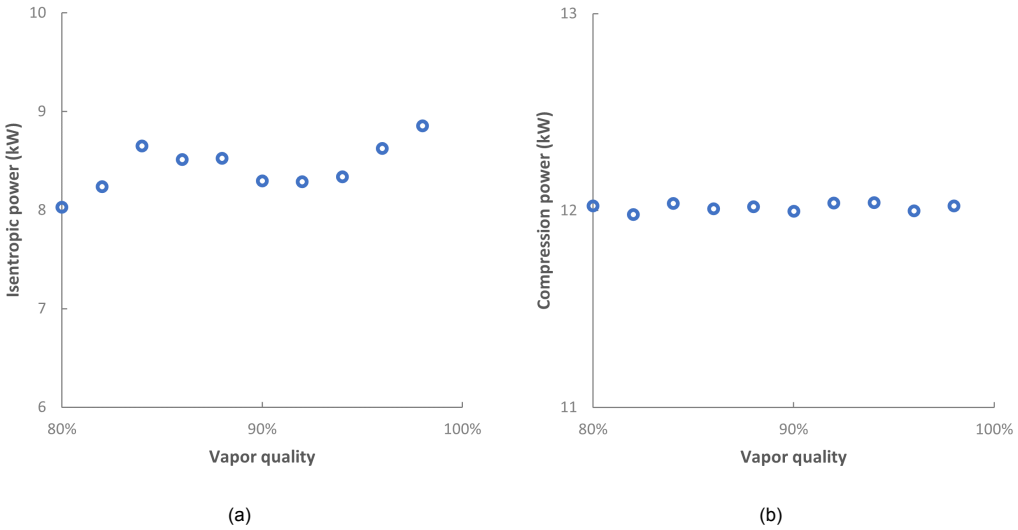

Figure 7.4: (a) Isentropic power and (b) real compression power as a function of the inlet vapor quality.

The isentropic power (Eq. 5.30) is a function of the mass flow rate in the compressor and of the isentropic enthalpy difference ($h_{2s} - h_1$). The isentropic enthalpy difference increases linearly with the vapor quality (Figure 7.5b). When less liquid is available to cool down the vapor, its temperature will rise, reaching the superheated state. In the two-phase zone, the enthalpy difference between the suction and the discharge state is significantly smaller compared to the superheated zone.

Based on these last statements, a linear increase of the isentropic efficiency with the rise of the inlet vapor quality would be expected. However, when the inlet vapor quality is increased, the compressor draws in less mass because of the reduced density of the mixture, which results in a reduction of the isentropic power (Figure 7.5a). The reduction in efficiency with an increase in vapor quality can also be substantiated by assuming that the liquid effectively seals a portion of the leakage paths. When the liquid content decreases, it leads to a reduction in mass within the volume cavity, due to the intensification of the leakages. Beyond a certain threshold ($Q_{suc} = 88\% - 90\%$), the increase in the variation of the specific enthalpy between inlet and outlet conditions is predominant, thus increasing the isentropic efficiency.

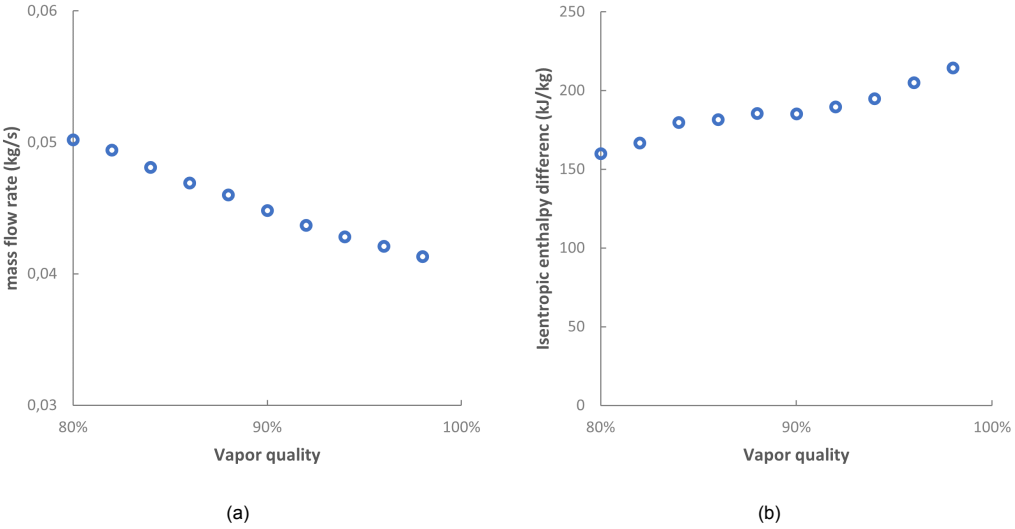

Figure 7.5: (a) Mass flow rate and (b) isentropic enthalpy difference as a function of the inlet vapor quality.

The isentropic efficiency's behavior can also be explained by the following phenomenon. As the vapor content at the suction increases, for the same inlet conditions (p_{suc} and T_{suc}), the ammonia concentration increases. This has a substantial impact on the thermodynamic behavior of the mixture. At lower concentrations the working fluid exhibits a wider two-phase region on the Temperature-Enthalpy diagram. When the ammonia concentration increases, the mixture approaches a state where the two-phase region narrows. This behavior is associated with the reduced enthalpy changes. Simultaneously, when increasing the ammonia concentration, the temperature glide in the two-phase region increases, leading to higher changes in enthalpy difference.

In summary, the decrease in isentropic efficiency with increasing ammonia concentration can be a consequence of the narrowing of the two-phase region, reducing the enthalpy changes. While the increase in isentropic efficiency with increasing ammonia concentration can be a consequence of the increase in temperature glide of the mixture in the two-phase region. Furthermore, it is important to take into account the alterations in the thermophysical properties of the ammonia-water mixture when changing the ammonia concentration.

Figure 7.6 illustrates both the discharge temperature of the mixture (in blue) and the corresponding saturation temperature (in green) as a function of the inlet vapor quality. For vapor qualities lower than 88%, the working fluid remains in a two-phase state, resulting in outlet vapor qualities ranging from 71% to 94%. When the inlet vapor quality reaches 90% or higher, the mixture at the discharge becomes superheated vapor. At 90% vapor quality, the superheat is approximately 4 °C, but as the inlet vapor quality increases, it can reach high values up to 30 °C. Therefore, it is crucial to note that even though

the isentropic efficiency increases beyond a certain threshold with higher inlet vapor qualities, the level of superheat also rises significantly.

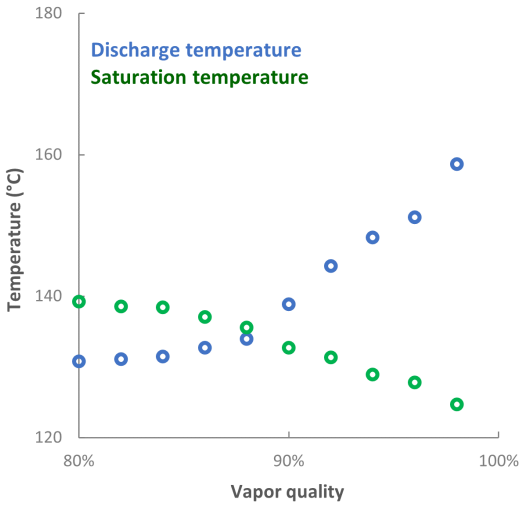

Figure 7.6: Discharge and saturation temperatures as a function of the inlet vapor quality.

Before reaching conclusions, it is important to assess the impact of the inlet vapor quality on the system performance. Figure 7.7 illustrates the COP of the heat pump as a function of the inlet vapor quality. The COP initially rises until reaching a maximum value before declining. This behavior aligns with the factors impacting the isentropic efficiency. Given that the compression power remains relatively constant, the largest influence arises from the heat transfer in the absorber, which is a function of the system flow rate and of the variation in enthalpy between the inlet and the outlet (as described in Eq. 5.38).

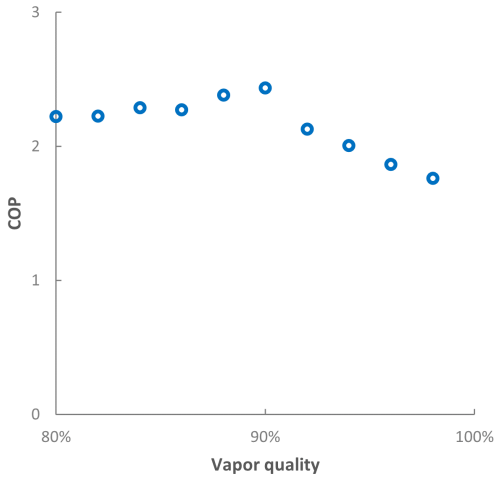

Figure 7.7: COP as a function of the inlet vapor quality.

The mass of the system decreases linearly when increasing the inlet vapor quality. This behavior originates from two factors: the decrease in the mixture density due to higher vapor content (Figure 7.8a) and the increase in mass from the gap seal. Differently, the variation in enthalpy exhibits two distinct behaviors, which resemble the behaviors of the COP (Figure 7.8b). Initially, the enthalpy variation increases for the reasons previously mentioned. Subsequently, it relatively stays constant due to changes in the thermodynamic properties of the mixture. As previously explained, increasing the vapor content causes the Temperature-enthalpy curve to contract, leading to reduced variation in specific

enthalpy. Simultaneously, increasing the ammonia concentration, the temperature glide inside the absorber increases. These two phenomena counterbalance each other, resulting in a negligible variation in the enthalpy difference. In conclusion, initially the COP is influenced by the significant variation in enthalpy difference. After reaching a certain threshold, the thermodynamic properties change, resulting in a relatively constant enthalpy variation. At this point, the reduction of the cycle flow rate becomes predominant, causing a decrease in the COP.

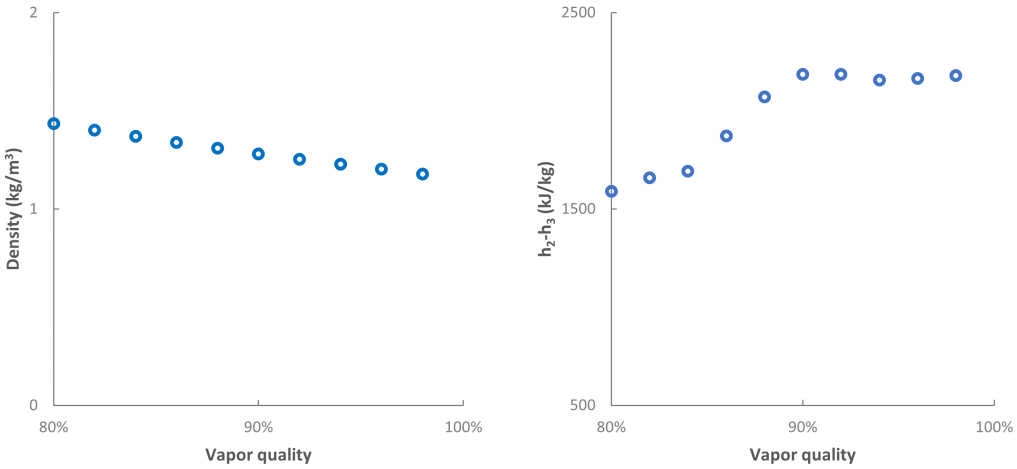

(a) (b)

Figure 7.8: (a) Density of the mixture and (b) enthalpy difference at the absorber as a function of the inlet vapor quality.

In Figure 7.9, the volumetric efficiency is plotted as a function of the inlet vapor quality. While the volumetric efficiency is less affected by changes in vapor quality compared to isentropic efficiency, it does exhibit a slight decrease with higher vapor qualities. This decrease can be attributed to the reduced volume flow drawn in by the compressor as the vapor content increases. As mentioned earlier, even though the mass decreases, the specific volume of the mixture increases with higher ammonia content and higher suction temperatures. These two factors partially offset each other, making the volumetric efficiency less sensitive to changes in the inlet vapor quality. However, the overall volumetric efficiency still decreases due to the greater impact of the mass reduction.

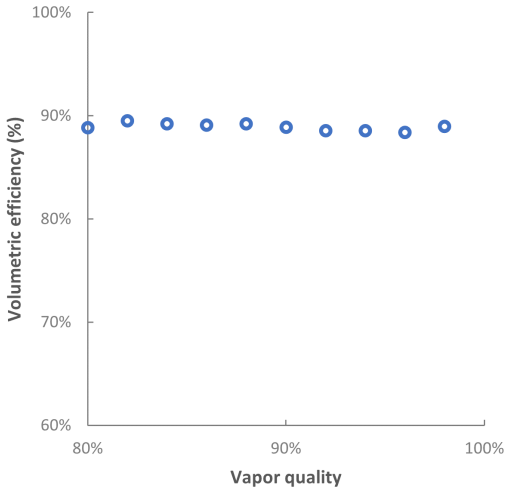

Figure 7.9: Volumetric efficiency as a function of the inlet vapor quality.

7.3. Investigation on the impact of the mass from the gap seal

Allowing a back flow from the gap seal can be a method to reduce leakages from the high pressure side to the low pressure side. This flow is re-injected at the inlet of the compressor, leading to a mass recovery. Relatively few studies were performed on this matter. In the experimental study of Kothari (2020), this flow was unrestricted and its value was related exclusively to the difference in pressure between discharge and suction, the cross-sectional area of the tube and the density of the vapor. For the experiments that were planned during this master thesis, a needle valve and a pressure gauge were placed on this pipe to control the flow. The purpose was to investigate the impact that the mass from the gap seal, hereafter referred to as $\dot{m}_{seal}$, has on the compressor's performance. Due to the aforementioned reasons, the experimental study was not carried out, and the investigation was rather performed digitally using the *compressor model*. The following case was tested:

Table 7.1: Operating conditions used in the investigation of the flow from the gap seal.

p_{suc} [bara]	PR	T_{suc} [°C]	X_{suc} [kg/kg]
2	3	78.5	0.54

During the investigation, these conditions were kept constant for the flow coming from the rest of the system, however, the input parameters for the compressor changed according to the value of $\dot{m}_{seal}$ and its impact on the rest of the flow. For this case, $\dot{m}_{seal}$ was computed as if the flow was unrestricted (100%). Then this flow was reduced with a step size of 10% until reaching a zero $\dot{m}_{seal}$. In an experimental setup, this condition would not be reachable since the gap seal would collapse. In order to obtain the input conditions for the *compressor model*, another side model was developed.

In Figure 7.10, the isentropic efficiency is plotted as a function of the fraction of $\dot{m}_{seal}$. It can be observed that the isentropic efficiency is highest when considering $\dot{m}_{seal}$ equal to 70% of the total $\dot{m}_{seal}$. For lower percentages, the isentropic efficiency drops, while for higher percentages it slightly decreases. In order to explain this behavior the isentropic compressor power and the real compressor

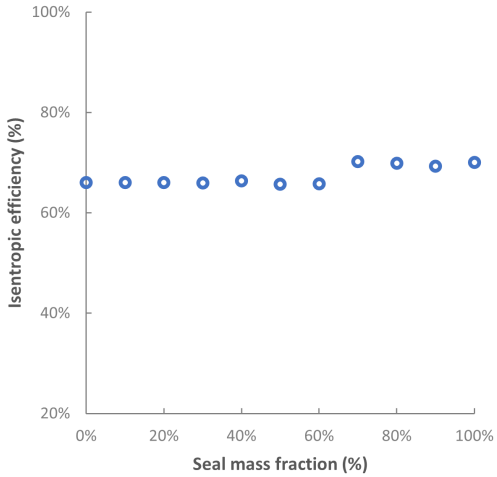

Figure 7.10: Isentropic efficiency as a function of the flow fraction from the gap seal.

power were analyzed. In Figure 7.11a and in Figure 7.11b, the isentropic compression power and the real compression power are plotted as a function of the fraction of $\dot{m}_{seal}$. The significant increase of the isentropic efficiency from 60% to 70% of the total $\dot{m}_{seal}$ is supported both by the drop of the real compression power and by the increase of the isentropic power in this range. However, it can be noticed that the isentropic power has the largest impact on the isentropic efficiency.

As previously explained, the isentropic power depends on the mass flow rate drawn in by the compressor and the isentropic specific enthalpy difference between the inlet and the outlet. The mass flow rate decreases when increasing the re-circulation of the flow from the gap seal (Figure 7.12b), while the isentropic specific enthalpy difference increases (Figure 7.12a).

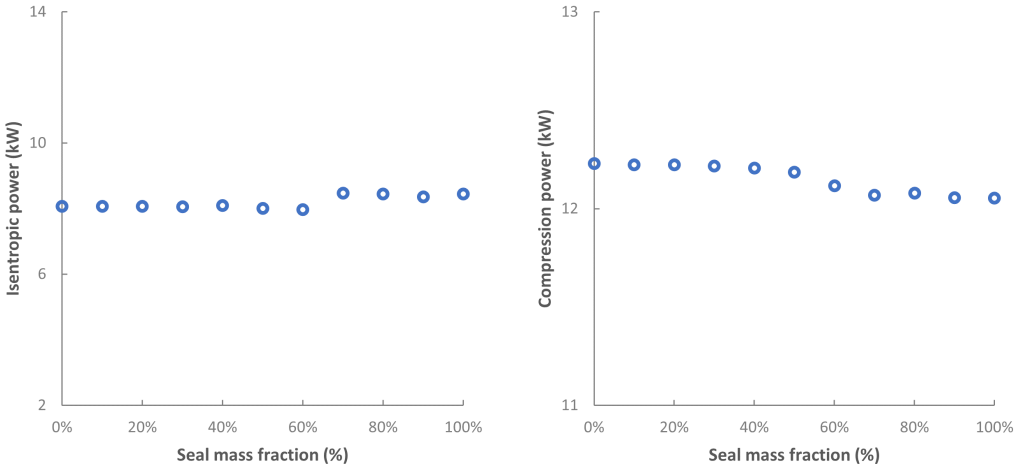

(a) (b)

Figure 7.11: (a) Isentropic power and (b) real compression power as a function of the flow fraction from the gap seal.

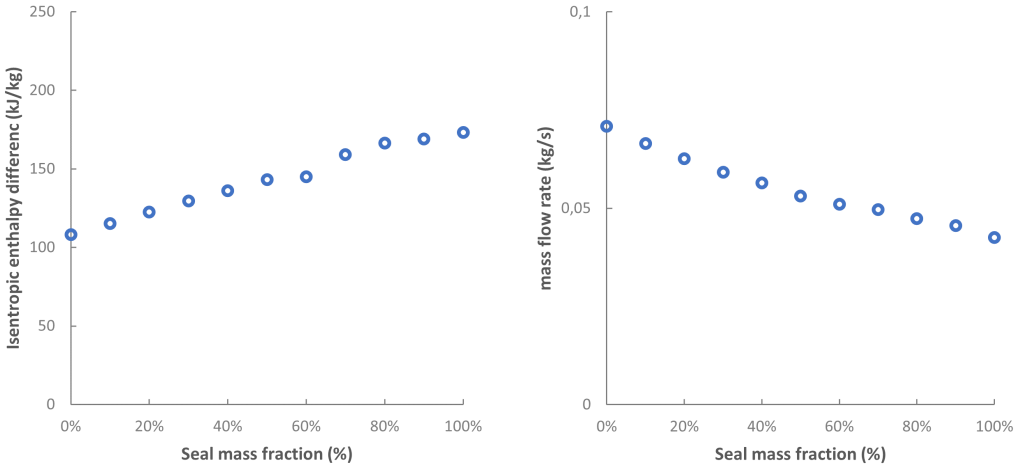

(a) (b)

Figure 7.12: (a) Isentropic enthalpy difference and (b) suction mass flow rate as a function of the flow fraction from the gap seal.

When increasing $\dot{m}_{seal}$ from zero, the increase in the isentropic specific enthalpy difference is comparable to the reduction of the mass flow rate drawn in by the compressor. When increasing the vapor content in the compressor, not only the density of the mixture decreases - leading to a lower mass flow rate - but also the difference in isentropic specific enthalpy difference increases, since the discharge point moves closer to superheated zone. The isentropic efficiency reaches its maximum when 70% of the total $\dot{m}_{seal}$ is employed. At this value, there is a noticeable change in the rate of mass flow rate reduction. This change is attributed to alterations in the thermodynamic properties of the mixture that occur when the ammonia content increases.

Figure 7.13 illustrates the density of the mixture as a function of $\dot{m}_{seal}$. The variation in density exhibits two distinct behaviors: initially, the rate of density reduction is very high, until it stabilize at a lower rate. This stabilization point occurs at 70% of the total $\dot{m}_{seal}$, which corresponds to the point where the isentropic efficiency increases.

Although the highest isentropic efficiency occurs at high $\dot{m}_{seal}$, the latter has a negative effect on the overall performance of the system. In Figure 7.14, the COP of the heat pump is plotted as a function of $\dot{m}_{seal}$. Increasing the re-circulation of the vapor in the compressor leads to lower mass flow rate in the

rest of the cycle significantly reducing the heat output, while the compressor power slightly reduces.

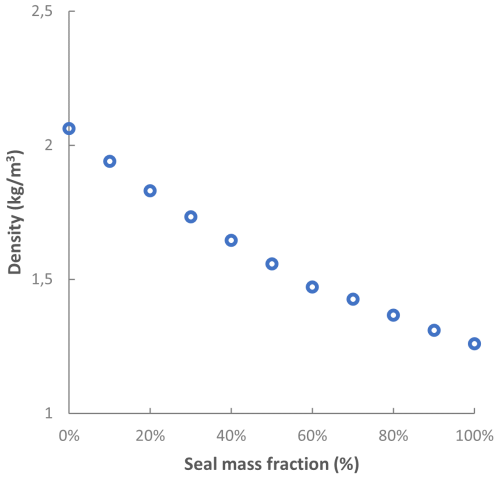

Figure 7.13: Density of the mixture as a function of the flow fraction from the gap seal.

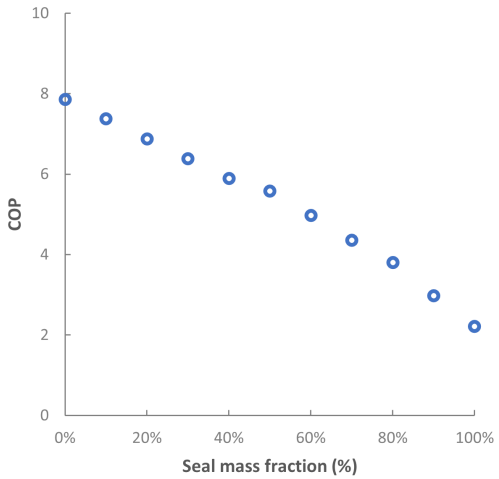

Figure 7.14: COP as a function of the flow fraction from the gap seal.

The volumetric efficiency remains relatively constant for $\dot{m}_{seal}$ values below 50%, however, it increases for higher values (Figure 7.15). This behavior can be attributed to the previously discussed phenomenon: as the vapor content increases, the mass decreases, but the specific volume of the mixture increases. For $\dot{m}_{seal}$ values exceeding 50%, the increase in mixture specific volume becomes the dominant factor overcoming the reduction in mass due to the substantial increase in ammonia fraction.

Overall, the impact of $\dot{m}_{seal}$ on the isentropic and volumetric efficiency is minimal from 0% to 60%, while it increases between 70% and 100%. However, it is necessary to consider the effect that $\dot{m}_{seal}$ has on the system.

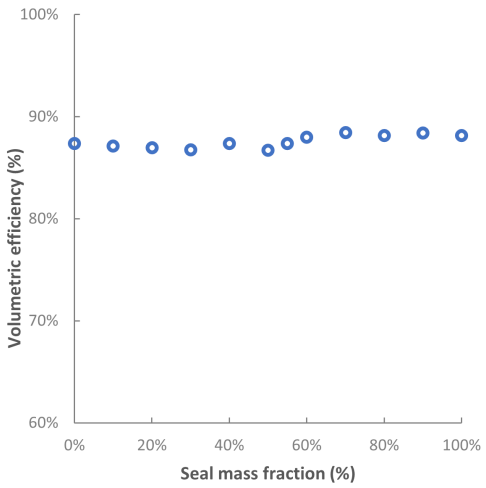

Figure 7.15: Volumetric efficiency as a function of the flow fraction from the gap seal.

8

Case Study

In this chapter, the developed digital CRHP is employed in the context of a real-life application. The potential available waste heat was estimated to be 100 PJ per year in the Netherlands [Schepers and Van Lieshout (2011)]. Despite a large amount of waste heat, the applications in which this energy is used in the Netherlands are very limited. The low temperatures of these streams discourage their recover due to the lack of applications performed at low temperatures. However, an interesting solution would be using these streams as a heat source to achieve higher temperatures. In the Food & Beverage industry, several operations require temperatures below 200°C. Among these, the Netherlands is the fourth largest dairy producer in EU [in Data (2023)]. As expected, a significant contribution to the energy consumption and to the generation of waste heat originates from the dairy industry. In this chapter, the amount of waste heat which would be recovered and produced by the digital heat pump is evaluated in the context of the dairy industry.

8.1. Recovery of waste heat in dairy industry

In 2019, the Netherlands produced 14 million tonnes of milk products [Hospers et al. (2022)].For each liter of milk, an estimated 0.2 to 10 liters of water are required, leading to the generation of large amounts of wastewater streams. [Vourch et al. (2008)]. Specifically, cleaning in process operations are estimated to account for 50% to 95% of the total wastewater volume [Daufin et al. (2001)]. These streams are discharged at temperatures between 70°C and 90°C, depending on the operations, thus they contain a significant amount of energy. The recovery of these temperatures might not be economically justified due to the limited occurrence of processes operating below 80°C. However, these wastewater streams can serve as a foundation for achieving higher temperatures required in essential processes, such as:

- Pasteurization: this process is employed to eliminate pathogens in the milk and it can be carried out at different temperatures. At 130°C ultra-pasteurization is performed, while at 100°C Higher-Heat shorter time pasteurization occurs.
- Sterilization: this process is an essential step for ensuring a long shelf life for liquid milk products. It typically occurs at temperatures between 120°C-135°C for very short time. It can be accomplished through steam injection or indirect contact heat transfer.
- Drying: this process transforms liquid milk into a powder form. Fluidized bed drying is commonly applied at temperatures between 80°C to 120°C. The secondary fluid heated is air.
- Baking: this process is used in cheese production. Baking involves oven temperatures that can vary between 100°C and 180°C. The heat pump has the potential to provide a significant amount of energy to preheat the oven.

If the electrical energy for the compressor is supplied by renewable sources, the heat pump could be considered a clean system with minimal emissions. The waste heat, which would be otherwise be dissipated into the environment or would necessitate additional cooling of the water streams, can be

recovered fully. This recovery allows to achieve higher temperatures that would otherwise be generated using fuel-based systems. From an energetic perspective, the recovery of waste heat for other critical applications already justifies the use of a high temperature heat pump. However, it is equally crucial to assess this means from an economic perspective.

8.2. Case study data

The findings discussed in Chapter 7 were applied to a real-case study. In the milk production process, wastewater streams are tipically discharged at 85°C. The heat pump recovers the waste heat using a heat exchanger, elevating it to higher temperatures. For instance, pressurized water at 3 bara and 20 °C needs to be heated to 125°C to perform sterilization operations. Table 8.1 presents the input data for the *compressor model*. In the course of this investigation, the mechanical efficiency of the compressor is maintained at a constant value of 77% and the motor efficiency at 93%. It is important to keep in mind that these input data have already taken into account the influence of the flow coming from the gap seal.

Table 8.1: Input data for the compressor used for the case study.

n [rpm]	p_{suc} [bara]	PR	% m_{seal}	% Q_{suc}
10320	2	3	70	90

The thermodynamic points along the heat pump cycle are presented in Table 8.2 and in Figure 8.1, which shows the Temperature-specific enthalpy plot. Figure 8.1 demonstrates that at the same pressure, the saturation temperature is not constant, but it exhibits a significant temperature glide. This characteristic would be beneficial when transferring heat using a fluid with a similar temperature glide.

Table 8.2: Thermodynamic states of the heat pump.

p_{low} [bara]	p_{high} [bara]	T_1 [°C]	T_2 [°C]	T_3 [°C]	T_4 [°C]
2	6	80	138	27	0

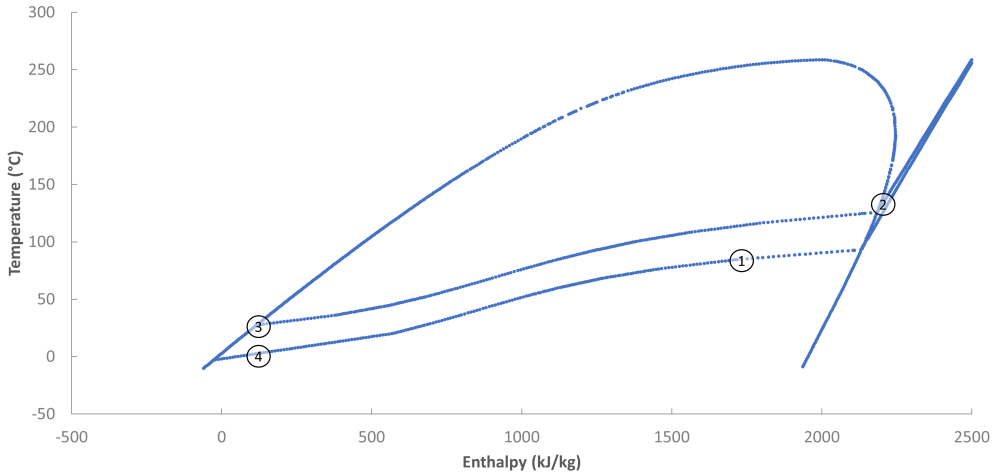

Figure 8.1: Temperature-specific enthalpy ($T - h$) plot for the thermodynamic cycle used for the case study.

In Table 8.3, the performance indices and the specifications of both the compressor and the heat pump are shown.

Table 8.3: Specification of the heat pump and compressor.

η_{is}	η_{vol}	COP	$\dot{Q}_{sink}$ [kW]	$\dot{W}_{comp}$ [kW]	$\Delta T_{glide,sink}$ [°C]	$\Delta T_{glide,source}$ [°C]
0.69	0.88	3.46	44.97	13.00	97.36	80

Table 8.4 presents the specification for the secondary fluids. The water used at the heat sink is pressurized at 3 bara. The use of non-pressurized water at temperatures higher than 100°C would be unfeasible due to the phase change that occurs at constant temperature. The wastewater used at the heat source is at atmospheric pressure, since a phase change process does not occur.

Table 8.4: Secondary fluid specification at the heat sink and heat source.

p_{sink} [bara]	$\dot{m}_{water,sink}$ [kg/s]	$\Delta T_{glide,sink}$ [°C]	p_{source} [bara]	$\dot{m}_{water,source}$ [kg/s]	$\Delta T_{glide,source}$ [°C]
3	0.10	105	1	0.10	70

The CRHP for this application enables the recovery of 32 kW of heat, exchanging heat with 3.44 mega liters of wastewater streams per year. Considering the milk production of DOC KAAS B.V. in the Netherlands, the following two scenarios are compared:

- Best-case scenario: 0.2 liters of water per liter of milk are needed. DOC KAAS B.V. requires 6.60 mega liters of water per year for cleaning and other operations. This water has high energy content due to the high temperatures. The full amount of waste heat is estimated to be 61.34 kW.
- Worst-case scenario: 5 liters of water per liter of milk are needed. DOC KAAS B.V. requires 165 mega liters of water per year. The full amount of waste heat is estimated to be 1.5 MW.

Amounts of water larger than 5 liters per liter of milk have been excluded. The worst-case scenario is unlikely to happen. This amount of water was compared to the water use of a larger company in the Netherlands (Friesland Campina), which amounts to 4.2 mega liters. However, the worst-case scenario is still used as a reference. In the best-case scenario, a single heat pump would recover more than half of the waste heat (52%). In the worst-case scenario, a single heat pump would recover 2.14% of the waste heat. As mentioned before, this case is unlikely to happen, given the comparison with data sheets from a larger company. Therefore, it is expected that a single heat pump would recover at least 50% of the whole waste heat contained in water streams used in cleaning processes.

In both cases, the heat pump would raise the temperatures of the streams to higher values, up to 140°C. For this, 45 kW of heat would be delivered to perform the previously mentioned operations. Otherwise, this heat would likely be generated using fuel-based technologies, contributing to the environmental pollution. If the 13 kW of electricity needed for the compressor are generated through renewable sources, the heat pump can be considered a clean system, working with a natural fluid (GWP=0), which recovers heat which is essential for other operations. Even if this heat pump only recovers 50% of the total waste heat, it would still be possible to consider a larger heat pump or use multiple heat pumps. However, it is essential to assess the economic aspects before implementing multiple heat pumps. To fulfill this purpose, a general economical estimation for this system was conducted.

For the economical analysis, a fossil fuel-fired boiler was compared with the developed CRHP. The considered CRHP consists of two heat exchangers, one expansion valve and a twin-screw compressor. An additional pump is needed to pressurize the secondary fluid. The capital costs of each equipment were calculated. The costs of the expansion valve and of the pump can be considered negligible compared to the costs of the compressor and of the heat exchangers. The selected type of heat exchanger is a plate heat exchanger. Besides being the most cost-effective choice when working with fluids below 200°C and 1 MPa, this type is also ideal to minimize fouling. It is also easy to disassemble for regular maintenance [Shah and Sekulic (2003)]. The purchased equipment cost (PEC) of all the components was computed with the following formula:

$$PEC_Y = PEC_W \left(\frac{X_Y}{X_W} \right)^{\gamma} \tag{8.1}$$

where PEC_W is the cost at base capacity X_W and γ is the cost function exponent. The cost correlations for the heat exchangers and the compressor are provided by Jensen et al. (2015) and are shown in Table 8.5.

Table 8.5: Cost correlations for the components.Jensen et al. (2015).

Component	PEC_W [€]	X_W	γ
Heat exchanger	15,526	42 $[m^2]$	0.8
Electrical motor	10,710 · 2	250 $[kW]$	0.65
Compressor	11,914 · 2	178.4 $[m^3h^{-1}]$	0.66

The compressor and the electrical motor costs are multiplied by a factor of 2 to take into account the use of an oil-free compressor, which is known to be more expensive than an oil-lubricated compressor. Gudjonsdottir and Infante Ferreira (2020) claimed that the factor was advised by industrial partners of the project. The log mean temperature difference method is used for sizing the heat exchangers. The costs of the pump and of the valve are derived from a market analysis.

Table 8.6 shows the capital expenses (CAPEX) for each equipment of the heat pump.

Table 8.6: Investment costs for each component of the heat pump.

Absorber [€]	Desorber [€]	Compressor [€]	Electrical motor [€]	Pump & Valve [€]	Total [€]
1919.5	2194.8	20,448	3135	≈950	≈25,512

The total capital investment (TCI) of the CRHP, including installation costs, can be calculated with the following formula:

$$TCI_{HP} = 3.11 \sum PEC_k \tag{8.2}$$

The factor 3.11 was applied to consider additional costs related to the installation of the system at an existing facility. This factor includes costs such as: piping, electrical equipment, civil and structural work, construction work [van de Bor and Infante Ferreira (2013)]. The total installed cost of the CRHP amounts to 79,343 €.

When evaluating an industrial system, it is fundamental to consider the operating expenses (OPEX) and the CO_2 emissions. Apart from the maintenance costs, the OPEX associated with the heat pump consists primarily of the electricity required for the compressor. Considering the current electricity price in the Netherlands for non-household consumers [Department (2023)], the operating cost of the compressor amounts to 19,650 €/ year. The electricity cost of the pump was estimated to be 120 €/ year, which is negligible when compared to the compressor's OPEX. For this study, the maintenance costs were neglected.

Sterilization of milk products typically employs a gas-fired boiler for the process. Based on a market analysis, the estimated CAPEX for acquiring such a boiler is approximately 2500 €. However, it is assumed that the boiler is already installed at the facility, therefore the CAPEX and TCI are neglected. For this study, the boiler's efficiency is assumed to be 88%. To generate the same quantity of heat delivered by the heat pump, 32253 m^3 of gas are required. Considering the natural gas price in the Netherlands, the yearly operating costs for the boiler amount to 48,368 €/ year. An economic saving of 59.6 % in operating costs is achieved when employing the considered heat pump compared to the boiler.

The payback period (PBP) is the ratio between the total investment and the annual saving:

$$PBP = \frac{TCI_{HP}}{OPEX_{Boiler} - OPEX_{HP}} \tag{8.3}$$

The payback period for this heat pump is equal to 2.76 years; it can be considered relatively short for an industrial heat pump, indicating both energy savings and potential environmental benefits. From an environmental perspective, the gas-boiler would produce 100% more emissions, if the emissions for the

heat pump can be considered negligible. Considering the CO_2 emission factor for 2022 [Zijlema (2020)] the boiler would produce 104 tonnes CO_2 $year^{-1}$. In the context of future environmental regulations and emissions control mechanisms, such as carbon taxes or EU Carbon Permits, adopting a heat pump may present a cost-saving opportunity in the long run. The EU Carbon Permits are designed to incentives emissions reductions and negatively impact carbon intensive technologies. Considering the current EU carbon permits [LLC (2023)], the annual costs associated with CO_2 emissions for the company would amount to 10,000 €/ year. Estimating that approximately 7 boilers would be needed to cover the entire sterilization operations for this specific factory, the carbon emissions amounts to 728 tonnes / year, leading to 65,520 €/ year of carbon tax. In addition, it is crucial to consider that EU Carbon Permits are expected to continue rising, with an estimated increase of 13.4% already in the next 12 months. Figure 8.2 shows how the EU Carbon Permits have been drastically rising in the last 10 years.

Figure 8.2: EU Carbon Permits (EUR) in the last 10 years. Figure from LLC (2023).

Beyond the low payback period and the environmental benefits, the financial advantage of the heat pump becomes even more evident in a regulatory framework where carbon emissions come with a monetary cost.

9

Conclusions & Recommendations

In this chapter, the key conclusions drawn from the study will be presented, followed by the recommendations for future research on the subject. This study focused on the development of a twin-screw compressor model, working with ammonia-water mixture, in which the liquid and the vapor phase are assumed at non-equilibrium conditions. Non-equilibrium conditions imply that the liquid and vapor phase have different properties, e.g. different temperatures and ammonia concentrations; separate sets of governing equations are used for both phases. The governing equations are integrated with sub-models to calculate the heat transfer between the liquid and the vapor phases, which are in direct contact, and the leakages across the different paths. In this work the re-circulation of the mass coming from the gap seal is not neglected. This flow impacts both the inlet and outlet conditions of the compressor and the operating conditions of the rest of the system. For this purpose, the *compressor model* is integrated with other three additional models: the *input data model*, the *discharge pipe data model* and the *cycle model*. The first estimates the flow coming from the gap seal and it is used to get the right input conditions to give to the *compressor model*. The second simulates the heat transfer between the liquid and the vapor phase in the pipe after the compressor discharge; this model is used to obtain the temperature of the mixture when the liquid and the vapor returns at equilibrium conditions. The third is used to calculate the thermodynamic states along the cycle and the COP of the system. The models were validated with the experiments performed by Kothari (2020).

9.1. Conclusions

The models were used for the investigation of the best operating parameters to achieve the highest level of performance of the system at specific conditions. Based on the results from this investigation, the following conclusions can be drawn:

- The isentropic efficiency follows a parabolic trend when plotted as a function of the pressure ratio. The isentropic efficiency assumes the lowest values for the lowest pressure ratio (1.9) and the highest value for the design pressure ratio ($\approx$3). For higher pressure ratios (3.3 - 5.1) the isentropic efficiency decreases. The isentropic efficiency is highest for a rotational speed of 10320 rpm, while lowest for the highest rotational speed (12910 rpm).

- The volumetric efficiency curve shows a relatively flat profile with respect to the pressure ratio, indicating that it is not highly sensitive to changes in pressure ratio. The volumetric efficiency slightly decreases for higher pressure ratios (3.3-5.1). The volumetric efficiency is highest for a rotational speed of 10320 rpm, while lowest for the lowest rotational speed (9030 rpm).

- The trend of the isentropic efficiency as a function of the inlet vapor quality can be distinguished in two parts. In the first part, the isentropic efficiency decreases when increasing the vapor quality (82% - 90%), this behavior originates from the reduction of the flow drawn in by the compressor when increasing the vapor content of the incoming flow. In the second part, the isentropic efficiency increases when increasing the inlet vapor quality. This behavior originates from the increase of the isentropic enthalpy difference. When increasing the vapor content in the inflow, the

outflow is more near to the superheated zone, this implies higher variation in enthalpy between the inflow and the outflow. However, high inlet vapor qualities result in significant superheating.

- The COP exhibits a maximum for an inlet vapor quality of 90%.
- The isentropic efficiency is highest when the flow coming from the seal is equals to 70% of the total value as the flow was unrestricted. For lower values of $\dot{m}_{seal}$, the isentropic efficiency is much lower, while for higher value the isentropic efficiency slightly decreases.
- The volumetric efficiency is not dependent on $\dot{m}_{seal}$ below 50%, but it increases for higher values. The increase in ammonia content and suction temperature when increasing $\dot{m}_{seal}$ generates a slight increase in volumetric efficiency.
- The COP exhibits a linear decrease as the mass from the gap seal increases. This phenomenon occurs because a certain portion of the compressed mass does not continue to flow through the rest of the system. Consequently, there is a reduction in the heat output, although the compression power is only minimally affected.
- In the discussed case study, the heat pump demonstrates an ability to recover up to 50% of the waste heat. It has a low payback period and reduces operating expenses of 60% when compared to a traditional boiler. While the investment costs of the heat pump may surpass those of the boiler, this technology is essential for emission reduction. In the context of evolving environmental regulations, if carbon taxes are considered, a single boiler could potentially result in annual carbon taxes of 10,000 €.

9.2. Recommendations

In light of the analysis conducted in this study, several key recommendations can enhance the development and implementation of future models of compressors operating in wet compression conditions:

- To improve the accuracy of the model, it is necessary to acquire the geometrical data of the investigated compressor. These includes: the size of the ports, the opening and closing time of the ports, the wrap angle and the leakage paths. Future steps for this specific work should include the real data of the experimental compressor geometry into the model.
- For the purpose of this study, it would be valuable to conduct experiments on the behavior of the vapor and liquid phases when the mixture pressure is increased within a transparent viewing chamber.
- To better simulate the heat transfer between the vapor and liquid phases, specific correlations for the heat transfer coefficient for an ammonia-water mixture should be developed.
- A comparative analysis between the estimated mass flow rate from the gap seal and the experimental values is essential. Hence, new experiments should be conducted to measure the flow from the gap seal.
- To get more precise data for the compressor power and the efficiency, the development of separate model to account for heat and friction losses is fundamental.
- Additional temperature and pressure sensors should be installed both at the discharge and the suction side of the compressor. Ideally, two pair of sensors should be placed immediately after the discharge side of the compressor and another pair of sensors should be placed approximately 4 meters downstream from the discharge side. In this way the measurement and comparison of equilibrium temperatures with the model results for both discharge and equilibrium temperature can be done. At the suction side, it would be useful to place the sensors after the mass from the gap seal is injected.
- For the future implementation of CRHP in real-world applications, a comprehensive economic analysis should be conducted. This analysis should include maintenance costs, repair costs, employ salaries, taxes and incentives.

Bibliography

Ahrens, M. U., Hafner, A., & Eikevik, T. M. (2019). Development of ammonia-water hybrid absorption–compression heat pumps. *Proceedings of the 25th IIR International Congress of Refrigeration; IIF-IIR: Montréal, QC, Canada*, 4942–4949.

Ahrens, M. U., Loth, M., Tolstorebrov, I., Hafner, A., Kabelac, S., Wang, R., & Eikevik, T. M. (2021). Identification of existing challenges and future trends for the utilization of ammonia-water absorption–compression heat pumps at high temperature operation. *Applied Sciences*, *11*(10). https://www.mdpi.com/2076-3417/11/10/4635

Ahrens, M. U., Tolstorebrov, I., Tønsberg, E. K., Hafner, A., Wang, R., & Eikevik, T. M. (2023). Numerical investigation of an oil-free liquid-injected screw compressor with ammonia-water as refrigerant for high temperature heat pump applications. *Applied Thermal Engineering*, *219*, 119425.

Ayou, D. S. (2022). Double-lift ammonia/water compression-resorption heat pump for simultaneous industrial process heating and refrigeration applications. *19th International Refrigeration and Air Conditioning Conference at Purdue*, *2594*, 1–10.

Bianchi, G., Panayiotou, G. P., Aresti, L., Kalogirou, S. A., Florides, G. A., Tsamos, K., Tassou, S. A., & Christodoulides, P. (2019). Estimating the waste heat recovery in the european union industry. *Energy, Ecology and Environment*, *4*, 211–221.

Brückner, S., Liu, S., Miró, L., Radspieler, M., Cabeza, L. F., & Lävemann, E. (2015). Industrial waste heat recovery technologies: An economic analysis of heat transformation technologies. *Applied Energy*, *151*, 157–167.

Brunin, O., Feidt, M., & Hivet, B. (1997). Comparison of the working domains of some compression heat pumps and a compression-absorption heat pump. *International Journal of Refrigeration*, *20*(5), 308–318.

Chamoun, M., Rulliere, R., Haberschill, P., & Peureux, J.-L. (2013). Modelica-based modeling and simulation of a twin screw compressor for heat pump applications. *Applied thermal engineering*, *58*(1-2), 479–489.

Daufin, G., Escudier, J.-P., Carrère, H., Bérot, S., Fillaudeau, L., & Decloux, M. (2001). Recent and emerging applications of membrane processes in the food and dairy industry. *Food and Bioproducts Processing*, *79*(2), 89–102.

Department, S. R. (2023). Prices of electricity for non-household consumers in the netherlands from 2008 to 2022.

D.L.Thurrott. (2022). Atlas copco oil-free rotary screw compressors. https://dlthurrott.com/atlas-copco-oil-free-rotary-screw-compressors/

Ferreira, C. I. (2023). Experimental performance of a wet compressor operating with ammonia-water under high temperature compression-resorption heat pump conditions [unpublished manuscript].

Friedel, L. (1979). Improved friction pressure drop correlations for horizontal and vertical two-phase pipe flow. *European Two-Phase Flow Group Meeting, Ispra, Italy, paper E2.*

Gao, P., Qing, C., Chang, M.-M., Shao, L.-L., & Zhang, C.-L. (2020). Hybrid absorption-compression heat pump with two-stage rectification and subcooler. *Applied Thermal Engineering*, *181*, 116027.

Gudjonsdottir, V., & Infante Ferreira, C. I. F. (2020). Technical and economic analysis of wet compression–resorption heat pumps. *International Journal of Refrigeration*, *117*, 140–149.

Gudjonsdottir, V., Infante Ferreira, C. I. F., & Goethals, A. (2019). Wet compression model for entropy production minimization. *Applied Thermal Engineering*, *149*, 439–447.

Hospers, J., Kuling, L., Modernel, P., Lesschen, J. P., Blonk, H., Batlle-Bayer, L., van Straalen, W., & Dekker, S. (2022). The evolution of the carbon footprint of dutch raw milk production between 1990 and 2019. *Journal of Cleaner Production*, *380*, 134863.

in Data, O. W. (2023). Milk production [https://ourworldindata.org/grapher/milk-production-tonnes]. *Our World in Data*.

Infante Ferreira, C. I., Zamfirescu, C., & Zaytsev, D. (2006). Twin screw oil-free wet compressor for compression–absorption cycle. *International Journal of Refrigeration*, *29*(4), 556–565.

International Energy Agency. (2022a). *How to avoid gas shortages in the european union in 2023*.

International Energy Agency. (2022b). *World energy outlook*.

Itard, L. (1998). *Wet compression-resorption heat pump cycles. thermodynamic analysis and design* (Doctoral dissertation). Delft University of Technology.

Jensen, J. K., Ommen, T., Markussen, W. B., Reinholdt, L., & Elmegaard, B. (2015). Technical and economic working domains of industrial heat pumps: Part 2–ammonia-water hybrid absorption-compression heat pumps. *International Journal of Refrigeration*, *55*, 183–200.

Jung, C. W., Song, J. Y., & Kang, Y. T. (2018). Study on ammonia/water hybrid absorption/compression heat pump cycle to produce high temperature process water. *Energy*, *145*, 458–467.

Kim, J., Park, S.-R., Baik, Y.-J., Chang, K.-C., Ra, H.-S., Kim, M., & Kim, Y. (2013). Experimental study of operating characteristics of compression/absorption high-temperature hybrid heat pump using waste heat. *Renewable Energy*, *54*, 13–19.

Kothari, V. V. (2020). *Experimental validation of wet compression with a twin screw compressor prototype* (Master's thesis). Delft University of Technology.

Lemmon, E. W., Bell, I. H., Huber, M. L., & McLinden, M. O. (2018). NIST Standard Reference Database 23: Reference Fluid Thermodynamic and Transport Properties-REFPROP, Version 10.0, National Institute of Standards and Technology. https://doi.org/https://doi.org/10.18434/T4/1502528

LLC, M. (2023). *Eu carbon permits*. Retrieved September 6, 2023, from https://tradingeconomics.com/commodity/carbon

Markmann, B., Tokan, T., Loth, M., Stegmann, J., Hartmann, K.-H., Kruse, H., & Kabelac, S. (2019). Experimental results of an absorption-compression heat pump using the working fluid ammonia/water for heat recovery in industrial processes. *International Journal of Refrigeration*, *99*, 59–68.

Mikielewicz, D., & Wajs, J. (2019). Performance of the very high-temperature heat pump with low gwp working fluids. *Energy*, *182*, 460–470.

Panayiotou, G. P., Bianchi, G., Georgiou, G., Aresti, L., Argyrou, M., Agathokleous, R., Tsamos, K. M., Tassou, S. A., Florides, G., Kalogirou, S., et al. (2017). Preliminary assessment of waste heat potential in major european industries. *Energy Procedia*, *123*, 335–345.

Papapetrou, M., Kosmadakis, G., Cipollina, A., La Commare, U., & Micale, G. (2018). Industrial waste heat: Estimation of the technically available resource in the eu per industrial sector, temperature level and country. *Applied Thermal Engineering*, *138*, 207–216.

Rattner, A. (2017). Xnh3h2o ammonia-water thermodynamic mixture properties for matlab.

Schepers, B., & Van Lieshout, M. (2011). Ipo national roadmap waste heat. a quickscan of the options; ipo nationale routekaart restwarmte. een quickscan van de mogelijkheden.

Shah, R. K., & Sekulic, D. P. (2003). *Fundamentals of heat exchanger design*. John Wiley & Sons.

Tang, Y. (1995). *Computer aided design of twin screw compressors* (Doctoral dissertation). University of Strathclyde.

Thome, J. (2004). Wolverine tube heat transfer data book iii. wolverine tube inc.

van de Bor, D., & Infante Ferreira, C. (2013). Quick selection of industrial heat pump types including the impact of thermodynamic losses. *Energy*, *53*, 312–322. https://doi.org/https://doi.org/10.1016/j.energy.2013.02.065

Van De Bor, D., Infante Ferreira, C. I. F., & Kiss, A. A. (2014). Optimal performance of compression–resorption heat pump systems. *Applied thermal engineering*, *65*(1-2), 219–225.

Van de Bor, D., Infante Ferreira, C. I. F., & Kiss, A. A. (2015). Low grade waste heat recovery using heat pumps and power cycles. *Energy*, *89*, 864–873.

Vourch, M., Balannec, B., Chaufer, B., & Dorange, G. (2008). Treatment of dairy industry wastewater by reverse osmosis for water reuse. *Desalination*, *219*(1-3), 190–202.

Yanagisawa, T., Cheng, M., Fukuta, M., & Shimizu, T. (1990). Optimum operating pressure ratio for scroll compressor.

Zaytsev, D. V. (2003). *Development of wet compressor for application in compression-resorption heat pumps* (Doctoral dissertation). Delft University of Technology.

Zhang, J., Mondejar, M. E., & Haglind, F. (2019). General heat transfer correlations for flow boiling of zeotropic mixtures in horizontal plain tubes. *Applied Thermal Engineering*, *150*, 824–839.

Ziegler, F., & Riesch, P. (1993). Absorption cycles. a review with regard to energetic efficiency. *Heat Recovery Systems and CHP*, *13*(2), 147–159.

Zijlema, P. (2020). The netherlands: List of fuels and standard co2 emission factors version of january 2020.